MINISTÉRIO DA CIÊNCIA E TECNOLOGIA
INSTITUTO NACIONAL DE PESQUISAS ESPACIAIS

INPE-6532-PRP/211

PROJETO DE UM SISTEMA DE ESPALHAMENTO THOMSON PARA O TOKAMAK ETE

Primeiro Relatório de Atividades
Período : outubro/97 a dezembro/97

Luiz Angelo Berni

Relatório Técnico e Científico apresentado à FAPESP, referente à bolsa de Pós Doutoramento no país

INPE
São José dos Campos
1998

Ministério da Ciência e Tecnologia
Instituto Nacional de Pesquisas Espaciais

Segundo Relatório de Atividades

período : Outubro/97 a Dezembro/97

Bolsa de Pós Doutoramento no País - FAPESP

Projeto de um Sistema de Espalhamento Thomson para o Tokamak ETE

Processo 96/8819-1

Luiz Angelo Berni

INPE / LAP
São José dos Campos
1998

Resumo

Este relatório contém as atividades desenvolvidas no período de Outubro/97 a Dezembro/97 referentes ao processo 96/8819-1.

As propostas e sugestões para o sistema de coleção da luz espalhada no tokamak esférico ETE estão descritas no capítulo 1 . No capítulo 2 é sujerido a utilização do espalhamento Rayleigh para a calibração de todo o sistema ótico. Não foi possível testar o sistema de coleção por varredura no tokamak NOVA-UNICAMP devido a problemas com o sistema de vácuo da máquina. Parte destes testes (capítulo 3) foram realizados no próprio laboratório do grupo de plasma do INPE com o empréstimo de alguns componentes óticos cedidos pelo Prof. Dr. Munemasa Machida .

No início do segundo semestre de 1997 foram realizados testes de espalhamento com nitrogênio no tokamak NOVA-UNICAMP cujos resultados são apresentados no capítulo 4.

Um orçamento geral do sistema para o espalhamento Thomson no tokamak ETE é apresentado no capítulo 5.

Sumário

Apêndice

Capítulo 1

Sistema de Coleção de Luz Espalhada

Para coletar a luz espalhada no tokamak ETE foram propostos alguns sistemas. Nestes sistemas a quantidade de luz coletada foi maximizada, sendo que o espectrômetro (Jobin Yvon - HR640) é o elemento limitante com F/6,3 . Em todos os componentes é sujerido a utilização de filme anti-refletor do tipo HEBBAR (MellesGriot) reduzindo ao máximo as perdas por reflexão.

Na figura 1 está esquematizado o primeiro sistema proposto. Este sistema projeta a luz espalhada pelo plasma na fenda do espectrômetro utilizando três espelhos planos e uma ou um conjunto de lentes. O sistema de espelhos tem duas finalidades : 1- Serve para rodar a imagem em 90° permitindo um casamento perfeito entre o volume espalhador que está na horizontal com a fenda do espectrômetro na vertical; 2 - Através de um sistema manual ou eletrônico o primeiro espelho pode girar observando a luz espalhada ao longo do feixe do laser.

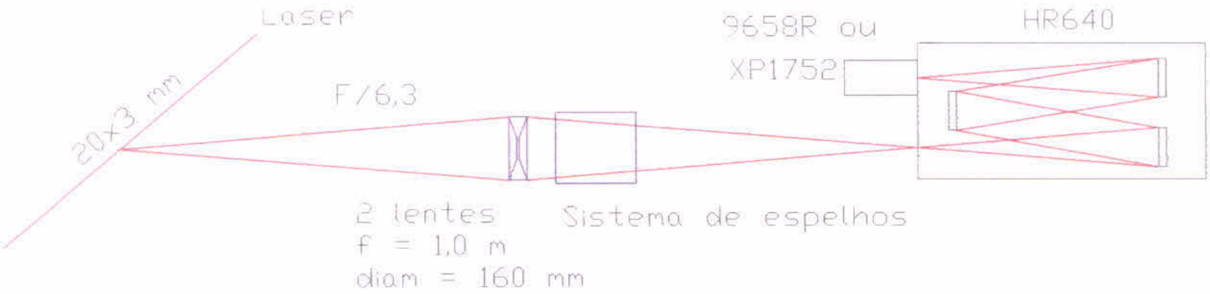

Figura 1.1 : Diagrama do sistema de coleção com espelhos.

Na figura 1.2 temos uma simulação deste sistema para o tokamak ETE. Esta simulação foi realizada utilizando o programa OPTICA (Mathematica) cuja listagem é fornecida no apêndice A1. Esta simulação foi realizada considerando os elementos óticos e equipamentos propostos para o ETE, a saber:

- Laser de rubi : 10 J; $\lambda = 694,3$ nm
- V1 : Volume espalhador , 20x3 mm
- L1, L2 : Lentes plano-convexas; f = 1,0 m; diam. = 16 cm
- E1 : Espelho plano 20x20 cm
- E2, E3 : Espelhos planos 10x10 cm

- Espectrômetro : Jobin Yvon HR640; F/6,3
- F1 :Fenda de entrada ,20x3 mm
- Detetores : 5 fotomultiplicadoras 9658R (THORN EMI) ou 1 fotomultiplicadora XP1752 (Philips).

Este sistema pode atingir uma transmissão de até 55%, se utilizados filmes anti-refletores adequados. Se considerarmos uma eficiência quâtica de 6 % poderam ser detectados até 3600 fotons no canal central. A maior dificuldade deste arranjo está no alinhamento crítico e na necessidade de se ter o espectrômetro junto a máquina. A lente utilizada para coletar a luz espalhada também é um elemento crítico. Para este sistema serão utilizadas duas lentes plano-convexas com os lados convexos em contato, diminuindo assim a aberração esférica. Uma lente ou conjunto de lentes especialmente projetada pode diminuir as perdas por aberrações, porém com um aumento considerável no custo.

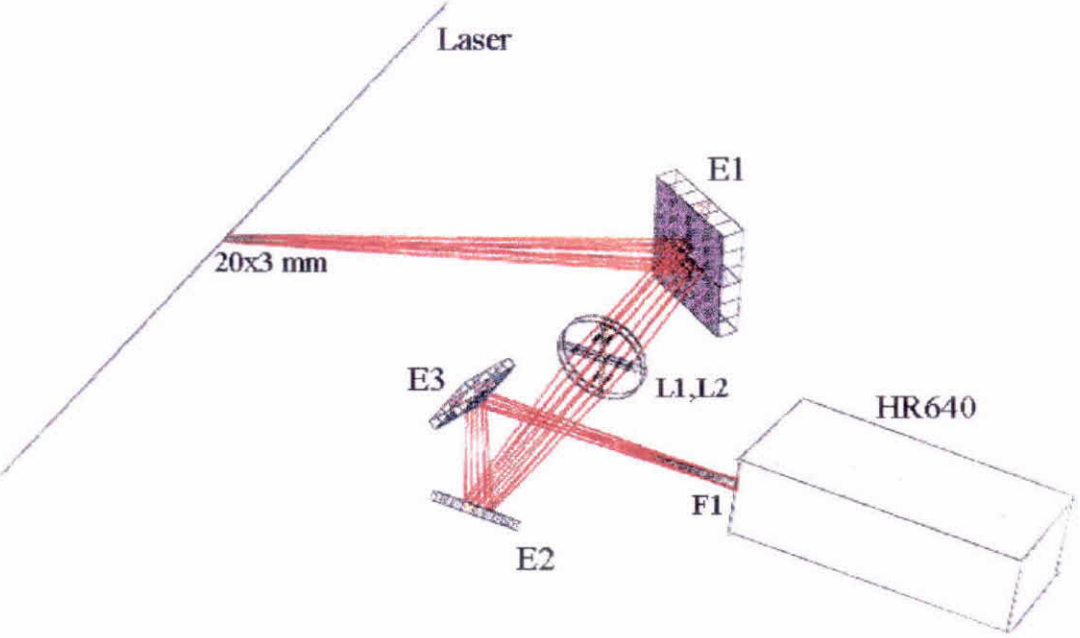

Figura 1.2 : Simulação do sistema de coleção com espelhos.

Sendo que a distância da luz espalhada em relação a lente coletora varia conforme o espelho móvel observa posições diferentes no plasma, ocorre uma perda de luz coletada devido a uma desfocalização da imagem na fenda de entrada do espectrômetro, como pode ser observado na figura 1.3 .

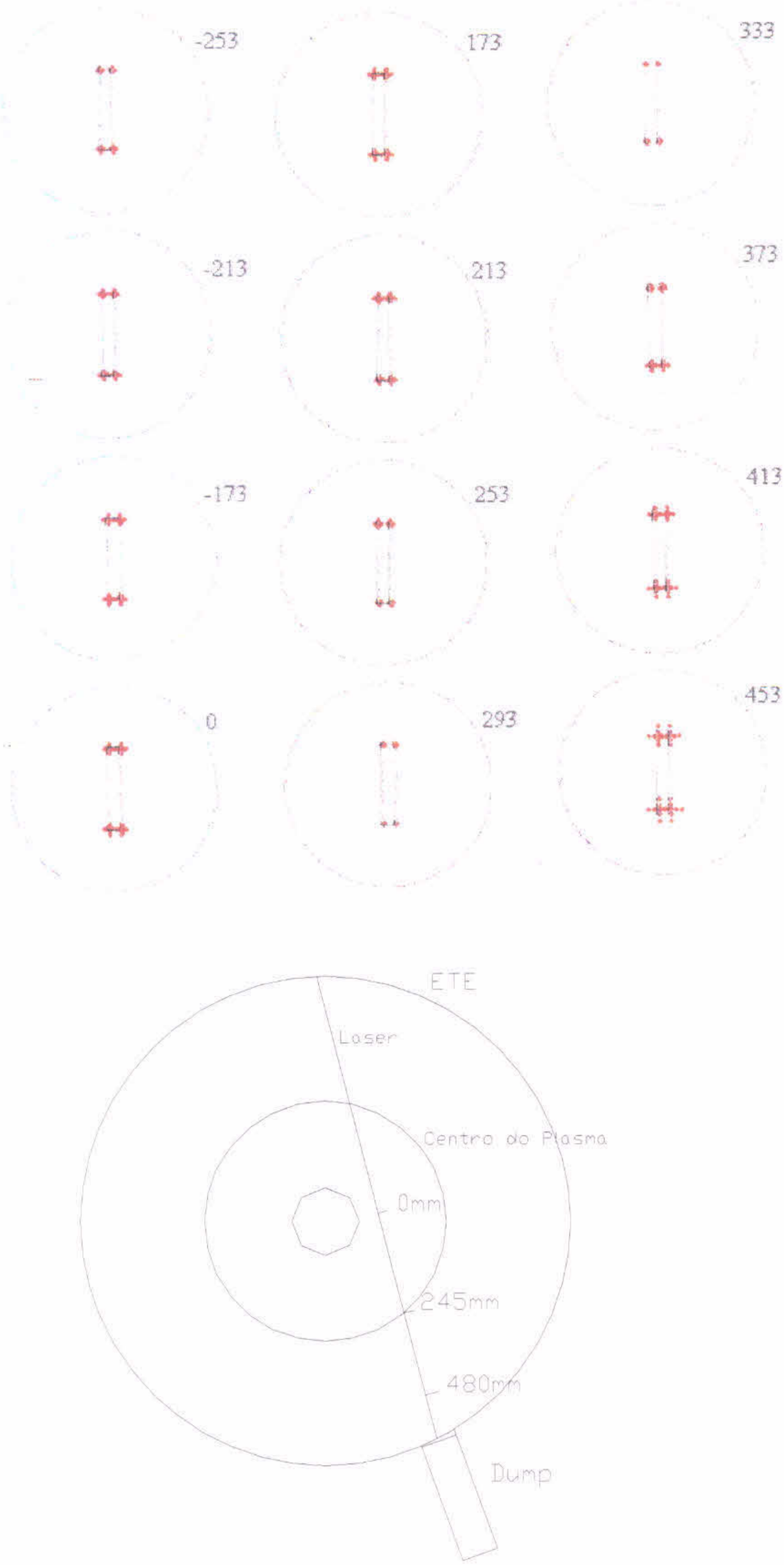

Figura 1.3 : Superior : projeção da luz espalhada na fenda de entrada do espectrômetro.
Inferior : posições de observação .

Observamos que para as posições compreendidas entre 213 mm e 373 mm temos a melhor focalização sendo que o máximo está em 333 mm. Para as regiões de borda (~ 453 mm) ocorrem as maiores perdas.

Na figura 1.4 temos a distribuição espectral da luz espalhada para vários valores de densidade e temperatura do plasma. As linhas verticais indicam as possíveis posições dos detetores. No caso de se utilizar 5 fotomultiplicadoras de canal simples deverão ser empregadas fibras óticas para o acoplamento espectrômetro-detetor. No caso da fotomultiplicadora multicanal XP1752 (ver apêndice A2) o detetor poderá ser acoplado diretamente ao espectrômetro. As posições geométricas dos detetores estão representadas na figura 1.5. Nesta figura foi considerada uma fenda de 20x3 mm.

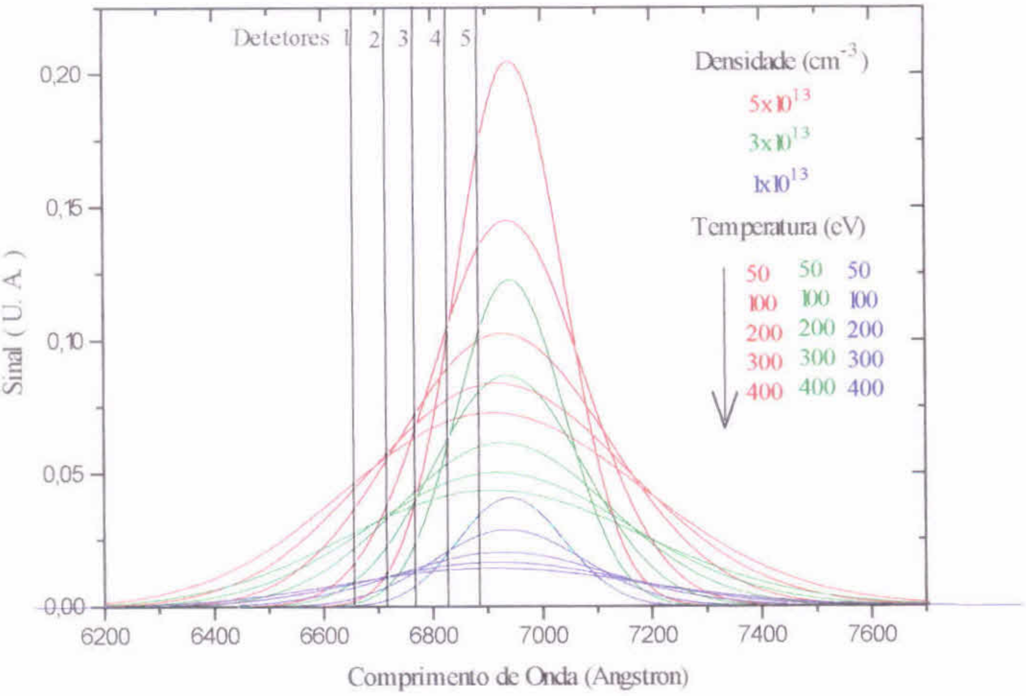

Figura 1.4 : Distribuição espectral da luz espalhada e posicionamento dos detetores.

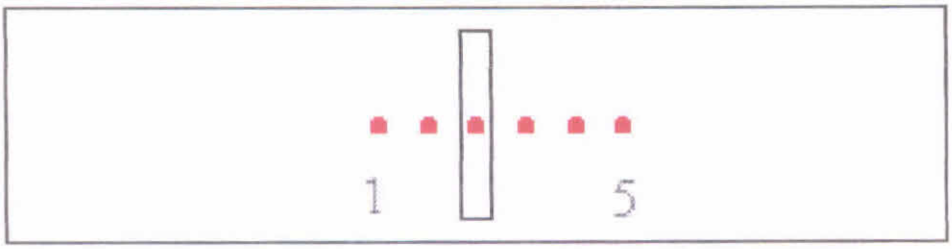

Posição	1	2	3	4	5	6
λ (Å)	6658	6716	6774	6831	6889	6943

Figura 1.5 : Fenda de saída e posicionamento dos detetores.

Nas figuras 1.6 e 1.7 estão representados os sistemas de coleção por fibras óticas. Na figura 1.6 temos um sistema de canal único que pode ser expandido para vários canais se for acrescentado fibras óticas no plano focal da lente coletora para cada região do plasma a ser observado. Neste sistema para cada canal são necessários um espectrômetro e detetores. O sistema por fibras óticas facilita o alinhamento e permite que o espectrômetro e detetores fiquem afastados da máquina, porém a transmisão máxima se reduz para 35 % o que significa 1400 fotons detectados no canal central. No sistema da figura 1.7 uma região maior do plasma (60 mm) é projetada na fenda de entrada do espectrômetro. Neste sistema pode-se utilizar uma única fibra coerente para transmitir a imagem ou três fibras incoerentes independentes. Neste caso a utilização de um detetor multicanal (XP1752) simplifica o sistema de deteção. Como a imagem projetada na fenda do espectrômetro representa três regiões do plasma temos que a quantidade de fotons cai para 260 por canal.

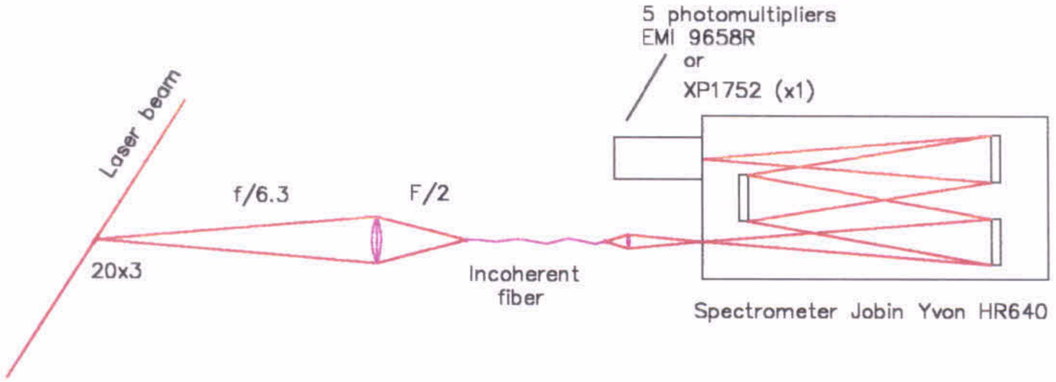

Figura 1.6 : Sistema de coleção por fibra ponto a ponto

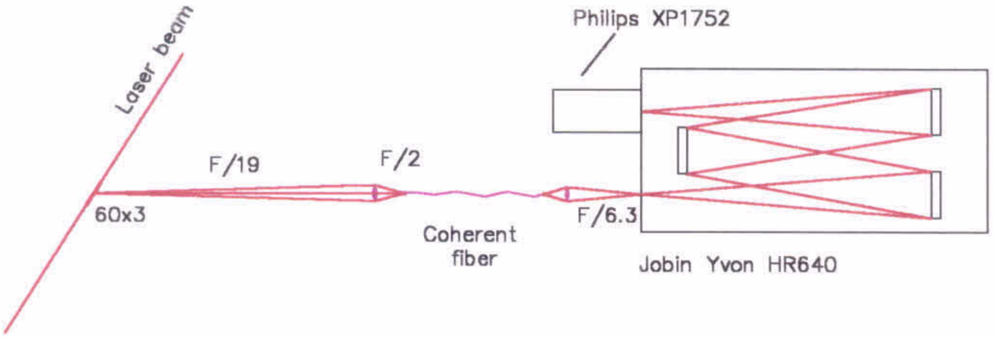

Figura 1.7 : Sistema multiposição de coleção por projeção

Capítulo 2

Método de Calibração do Sistema de Coleção

Como a temperatura do plasma é determinada pela largura do espectro espalhado, necessitamos calibrar o sistema de deteção (espectrômetro e fotomultiplicadora) em relação ao comprimento de onda. Enquanto para a obtenção da densidade do plasma todo o sistema de deteção incluindo a ótica devem ser calibrados em função da intensidade do sinal.

2.1 Calibração Relativa em Função do Comprimento de Onda

A intensidade do sinal na saída do espectrômetro em função do comprimento de onda pode ser calculada [Camp91] por :

$$I_s(\lambda_m) = \frac{1}{B_e}\int_{\lambda_m - \frac{B_e}{2}}^{\lambda_m + \frac{B_e}{2}} I_e(\lambda')d\lambda' \ , \qquad (2.1)$$

onde **$I_e(\lambda)$** e **B_e** são a intensidade do sinal e a largura espectral na fenda de entrada.

Para o detetor na saída do espectrômetro, a fenda de saída funciona como uma fonte. Assim o sinal medido pela fotomultiplicadora é a integral de **$I_s(\lambda)$** sobre a largura da fenda de saída **B_s**, ou seja :

$$S(\lambda_m) = \frac{C}{B_e}\int_{\lambda_m - \frac{B_s}{2}}^{\lambda_m + \frac{B_s}{2}}\int_{\lambda_m - \frac{B_e}{2}}^{\lambda_m + \frac{B_e}{2}} I_e(\lambda')d\lambda'd\lambda \ , \qquad (2.2)$$

onde **C** é uma constante relacionada com a sensibilidade do conjunto fotomultiplicadora e espectrômetro, ou seja, depende da transmissão (**τ**) do espectrômetro, do ganho (**G**) e da eficiência quântica (**η**) da fotomultiplicadora.

Se considerarmos que a intensidade da luz espalhada (**$I_s(\lambda)$**) seja constante na região $\lambda_m - \frac{B_s}{2} < \lambda_m < \lambda_m + \frac{B_s}{2}$, a equação (2.2) se reduz :

$$S(\lambda) = C \cdot I_s(\lambda) \cdot B_s \qquad (2.3)$$

A constante **C** pode ser medida com o auxílio da luz de uma lâmpada padrão. Porém, em geral, determina-se **C** por meio de espalhamento molecular como será descrito no próximo item . Ao realizar o espalhamento Thomson precisamos medir o sinal **$S(\lambda)$** em várias regiões do espectro. Como a resposta dos detetores não é constante ao longo do espectro, devemos fazer uma calibração relativa do sinal em relação ao comprimento de onda. Esta calibração pode ser feita com o auxílio da luz de uma lâmpada padrão difundida na fenda de entrada do espectrômetro.

A intensidade do espectro de uma lâmpada de tungstênio [Larr59] resulta em :

$$I = \int_{\Omega} \int_{A_e} L(\lambda, T) dA d\Omega = \Omega \cdot A_e \cdot L(\lambda, T) \tag{2.4}$$

onde : Ω : ângulo sólido de observação

A_e : área da fenda de entrada

$L = \dfrac{d^3 P}{dA d\lambda d\Omega \cos(\Theta)}$: radiância da lâmpada de tungstênio

Considerando que $L(\lambda,T)$ varie lentamente na região de interesse, podemos utilizar o mesmo raciocinio anterior,

$$S_{lamp}(\lambda_m) = Q(\lambda_m) \cdot L(\lambda_m, T) \tag{2.5}$$

onde : $Q(\lambda_m) = q(\lambda_m) \cdot B_s \cdot \Omega \cdot A_e$

$q(\lambda_m)$: constante relacionada com a sensibilidade da fotomultiplicadora

Fazendo-se uma varredura do sinal medido pela fotomultiplicadora para diversos comprimentos de onda e normalizando o sinal em relação ao comprimento de onda do laser de rubi ($\lambda_R = 6943$ Å), encontramos [Camp91] :

$$\begin{aligned}
S^n_{lamp}(\bar{\lambda}_1) &= \frac{Q(\bar{\lambda}_1)}{Q(\bar{\lambda}_R)} \cdot \frac{L(\bar{\lambda}_1, T)}{L(\bar{\lambda}_R, T)} = R(\bar{\lambda}_1) \cdot \frac{L(\bar{\lambda}_1, T)}{L(\bar{\lambda}_R, T)} \\
S^n_{lamp}(\bar{\lambda}_2) &= \frac{Q(\bar{\lambda}_2)}{Q(\bar{\lambda}_R)} \cdot \frac{L(\bar{\lambda}_2, T)}{L(\bar{\lambda}_R, T)} = R(\bar{\lambda}_2) \cdot \frac{L(\bar{\lambda}_2, T)}{L(\bar{\lambda}_R, T)} \\
S^n_{lamp}(\bar{\lambda}_3) &= \frac{Q(\bar{\lambda}_3)}{Q(\bar{\lambda}_R)} \cdot \frac{L(\bar{\lambda}_3, T)}{L(\bar{\lambda}_R, T)} = R(\bar{\lambda}_3) \cdot \frac{L(\bar{\lambda}_3, T)}{L(\bar{\lambda}_R, T)} \\
&\vdots \\
S^n_{lamp}(\bar{\lambda}_R) &= \frac{Q(\bar{\lambda}_R)}{Q(\bar{\lambda}_R)} \cdot \frac{L(\bar{\lambda}_R, T)}{L(\bar{\lambda}_R, T)} = 1 \\
&\vdots \\
S^n_{lamp}(\bar{\lambda}_N) &= \frac{Q(\bar{\lambda}_N)}{Q(\bar{\lambda}_R)} \cdot \frac{L(\bar{\lambda}_N, T)}{L(\bar{\lambda}_R, T)} = R(\bar{\lambda}_N) \cdot \frac{L(\bar{\lambda}_1, T)}{L(\bar{\lambda}_R, T)}
\end{aligned} \tag{2.6}$$

Através das relações (2.6) determinamos as constantes de calibração em função do comprimento de onda que devem ser incluídas na equação de espalhamento para se determinar o perfil espalhado, como apresentaremos mais adiante, no final deste capítulo.

4.2 - Calibração da Intensidade do Sinal

A temperatura do plasma pode ser conhecida apenas através do conhecimento da largura do espectro de espalhamento. Porém para se determinar a densidade necessitamos de uma calibração de sensibilidade do sistema de deteção. Na prática é comum utilizar uma das seguintes técnicas de calibração : calibração absoluta através de uma fonte padrão ou através dos espalhamentos Raman e Rayleigh.

Uma calibração absoluta do sistema para determinação da constante C pode ser feita através de uma fonte padrão . Com esta fonte podemos medir todos os parâmetros relacionados com a transmissão do sistema , a eficiência quântica e o ganho da fotomultiplicadora. O ângulo sólido e a região de observação podem ser calculados através de considerações geométricas. Além do mais é necessário medir a energia do laser a cada disparo, o que pode ser feito através de um fotodiodo calibrado. Esta técnica não é muito utilizada, pois apresenta muitas fontes de erros .

O espalhamento molecular é o mais empregado, porque utliliza a mesma ótica que o espalhamento Thomson eliminando os problemas de estimativa do volume espalhador e de perdas nos elementos óticos, calibração de detetores e medida de energia do laser. Este método de calibração consiste basicamente em colocar um gás conhecido sob uma determinada pressão na câmara de vácuo onde se produz o plasma. Através da medida do sinal espalhado pelas móleculas de gás pode-se calibrar o sistema de deteção, uma vez que conhecemos a densidade de gás utilizada. O espalhamento Raman é inelástico e consiste basicamente na mudança de estados vibracionais e rotacionais da molécula, gerando linhas espectrais em ambos os lados da freqüência da onda incidente, enquanto que o espalhamento Rayleigh é elástico e ocorre devido a oscilação dipolar da molécula na própria freqüência incidente. O espalhamento Raman, que apresenta uma intensidade 1000 vezes menor que o espalhamento Rayleigh [Long77], normalmente é empregado quando não se consegue reduzir a luz espúria a níveis suficientes.

No tokamak ETE pretende-se utilizar o espalhamento Rayleigh como método de calibração por ser mais preciso que a calibração por lâmpada padrão e mais intenso que o espalhamento Raman, para tanto o sistema de injeção e bloqueio da luz do laser foi cuidadosamente elaborado para manter os sinais espúrios o mais baixo possível (ver 1º relatório).

Uma vez que o espalhamento molecular Rayleigh apresenta características dipolares [Kunz68] podemos utilizar a mesma expressão de espalhamento para o calculo do perfil espalhado. Devido a baixa temperatura da molécula, o espectro espalhado resultante é sensivelmente mais estreito do que a largura do perfil instrumental, e está concentrado na região de comprimento de onda do laser. Se considerarmos o perfil de espalhamento do tipo maxwelliano, a potência espalhada por unidade de ângulo sólido integrada na freqüência, se reduz a :

$$\frac{dP_{Ray}}{d\Omega} = P_i \cdot \frac{d\sigma_R}{d\Omega} \cdot n_R \cdot L_s \qquad (2.7)$$

onde : **$d\sigma_R/d\Omega$** : seção de choque diferencial das moléculas do gás,

n_R : densidade de moléculas do gás.

O sinal Rayleigh medido pela fotomultiplicadora, integrado no ângulo sólido de observação Ω, é:

$$S_{Ray} = P_i \cdot \left(\frac{d\sigma_R}{d\Omega}\right)_{\Omega} \cdot n_R \cdot L_s \cdot \Omega \cdot \eta \cdot G \cdot \tau \qquad (2.8)$$

ou

$$L_s \cdot \Omega = \frac{S_{Ray}}{P_i \cdot n_R \cdot \left(\frac{d\sigma_R}{d\Omega}\right)_{\Omega} \cdot \eta \cdot G \cdot \tau}$$

Normalmente, nas medidas para se determinar o perfil espalhado Thomson evita-se a região central do espectro devido à forte influência de luz espúria. Desta forma o sinal medido por um detetor posicionado na N-ésima faixa de comprimento de onda a ser medida, com comprimento de onda médio **λ_N** (equação 2.3) em um ângulo sólido Ω, sem a componente iônica, se reduz a :

$$S_N(\lambda_N) = R_N \cdot B_s \cdot \frac{P_i \cdot r_o^2 \cdot c \cdot n_e \cdot L_s \cdot \Omega \cdot \eta \cdot G \cdot \tau}{2 \cdot \sqrt{\pi} \cdot \lambda_i \cdot \mathrm{sen}(\theta/2)} \cdot \left(1 - \frac{7 \cdot (\lambda_N - \lambda_i)}{2 \cdot \lambda_i}\right) \cdot \frac{1}{a} \cdot \left|1 - \frac{G_e}{\varepsilon}\right|^2 \cdot \exp\left(-\frac{c^2 \cdot (\lambda_N - \lambda_i)^2}{4 \cdot a^2 \cdot \lambda_i^2 \cdot \mathrm{sen}^2(\theta/2) \cdot \left(1 + \frac{(\lambda_N - \lambda_i)}{\lambda_i}\right)}\right) \qquad (2.9)$$

Substituindo (2.8) em (2.9), encontramos :

$$S_N(\lambda_N) = R_N \cdot B_s \cdot \frac{c \cdot n_e}{2 \cdot \sqrt{\pi} \cdot \lambda_i \cdot \mathrm{sen}({}^{\theta}\!/_{2})} \cdot \frac{S_{Ray}}{n_R} \cdot \frac{{}^{d\sigma_T}\!/_{d\Omega}}{{}^{d\sigma_R}\!/_{d\Omega}} \cdot \left(1 - \frac{7 \cdot (\lambda_N - \lambda_i)}{2 \cdot \lambda_i}\right) \cdot \frac{1}{a} \cdot \left|1 - \frac{G_e}{\varepsilon}\right|^2 \cdot \exp\left(-\left(\frac{c^2 \cdot (\lambda_N - \lambda_i)^2}{4 \cdot a^2 \cdot \lambda_i^2 \cdot \mathrm{sen}^2({}^{\theta}\!/_{2}) \cdot \left(1 + \frac{(\lambda_N - \lambda_i)}{\lambda_i}\right)}\right)\right) \qquad (2.10)$$

A razão $\mathbf{S_{Ray}/n_R}$ é obtida do gráfico de intensidade espalhada versus pressão do gás para o espalhamento Rayleigh. A razão entre as seções de choque Thomson e Rayleigh é tabelada para diversos gases [DeSi70]. Abaixo , na tabela 2.1 listamos alguns valores desta relação para alguns gases :

Gás	σ_T/σ_R
N_2	380
H_2	1769
CH_4	177
O_2	462

Tabela 2.1 : Razão entre as seções de choque Thomson e Rayleigh.

Para se verificar possíveis modificações no sistema ótico, devemos efetuar a calibração antes e depois do experimento.

Capítulo 3

Testes com o Protótipo do Sistema de Coleção por Varredura

No primeiro relatório foi apresentado o circuito eletrônico, o programa e os primeiros testes de posicionamento do sistema de coleção por varredura. Os testes finais seriam realizados junto ao grupo de plasmas da UNICAMP, porém devido a problemas com a bomba turbo molecular to tokamak NOVA-UNICAMP a máquina ficou parada por alguns meses. Por este motivo, parte dos testes finais foram realizados no próprio laboratório do grupo de plasma do INPE.

Na figura 3.1 temos uma fotografia da montagem experimental do sistema. Na parte inferior esquerda podemos ver o motor de passo com o espelho de varredura. No mesmo trilho deste espelho se encontra o restante da ótica de coleção. Na parte superior direita podemos ver o espectrômetro com a fotomultiplicadora. Na região central, em cima de um trilho, temos a fonte de luz para simular o espalhamento.

A simulação desta montagem está na figura 3.2 e os resultados na figura 3.3 . A curva teórica foi obtida das projeções da fonte de luz sobre a fenda do espectrômetro geradas pelo programa listado no apêndice A1. Verificamos que os dados apresentam uma boa concordância na região das posições negativas. Provavelmente, pequenos desalinhamentos de posicionamento devem explicar os sinais menores em relação a curva para as regiões positivas. Com esta simulação e com o experimento, verificamos que este sistema de coleção apresenta uma queda de até 40 % no sinal para as regiões afastadas da posição de focalização da lente coletora. Devemos lembrar que além dos problemas de aberração esférica , focalização da imagem sobre a fenda de entrada do espectrômetro, a intensidade no diagnóstico de espalhamento varia com o ângulo de coleção que pode aumentar ainda mais esta queda no sinal.

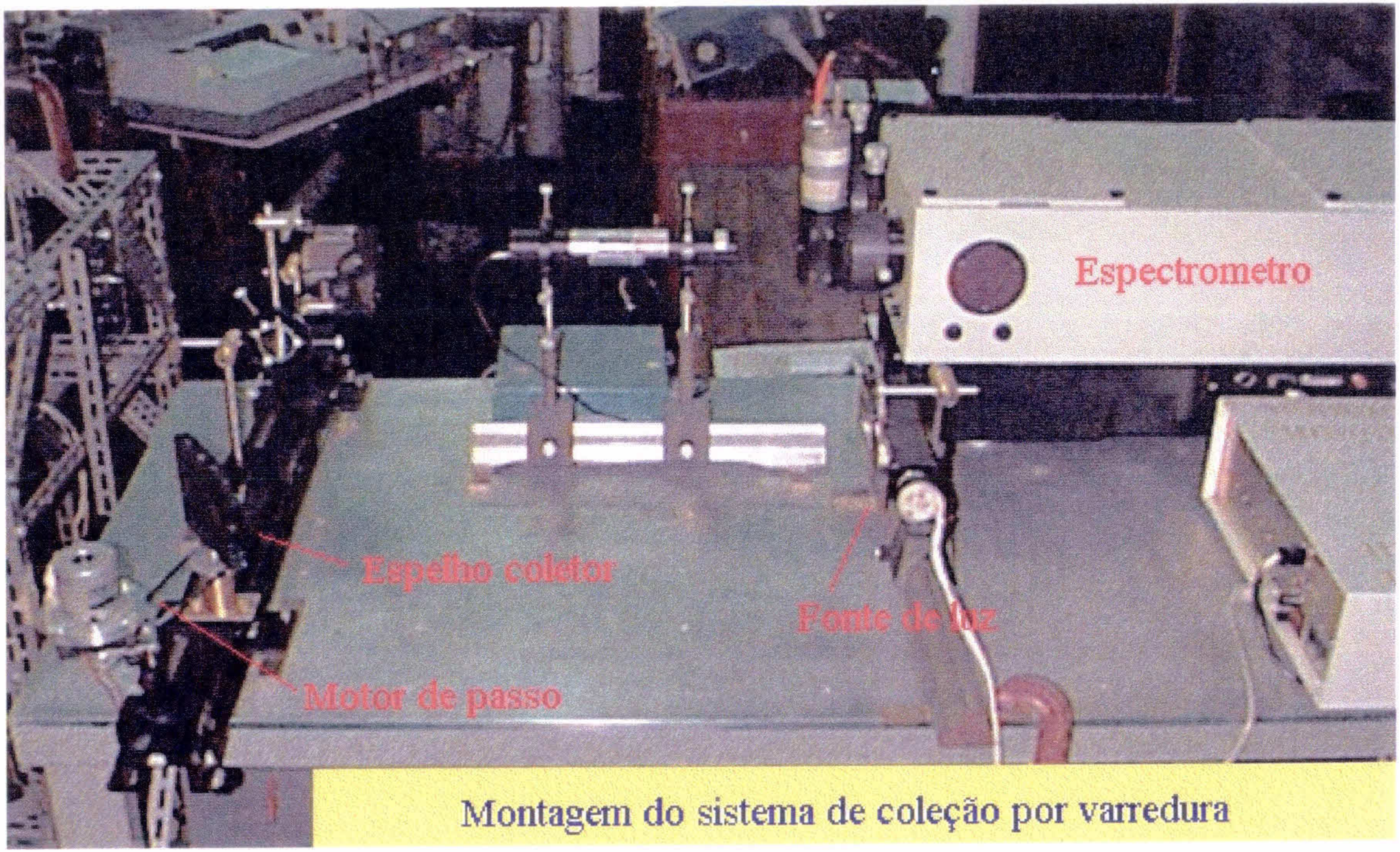

Figura 3.1 : Montagem da ótica de coleção para testes do sistema de varredura.

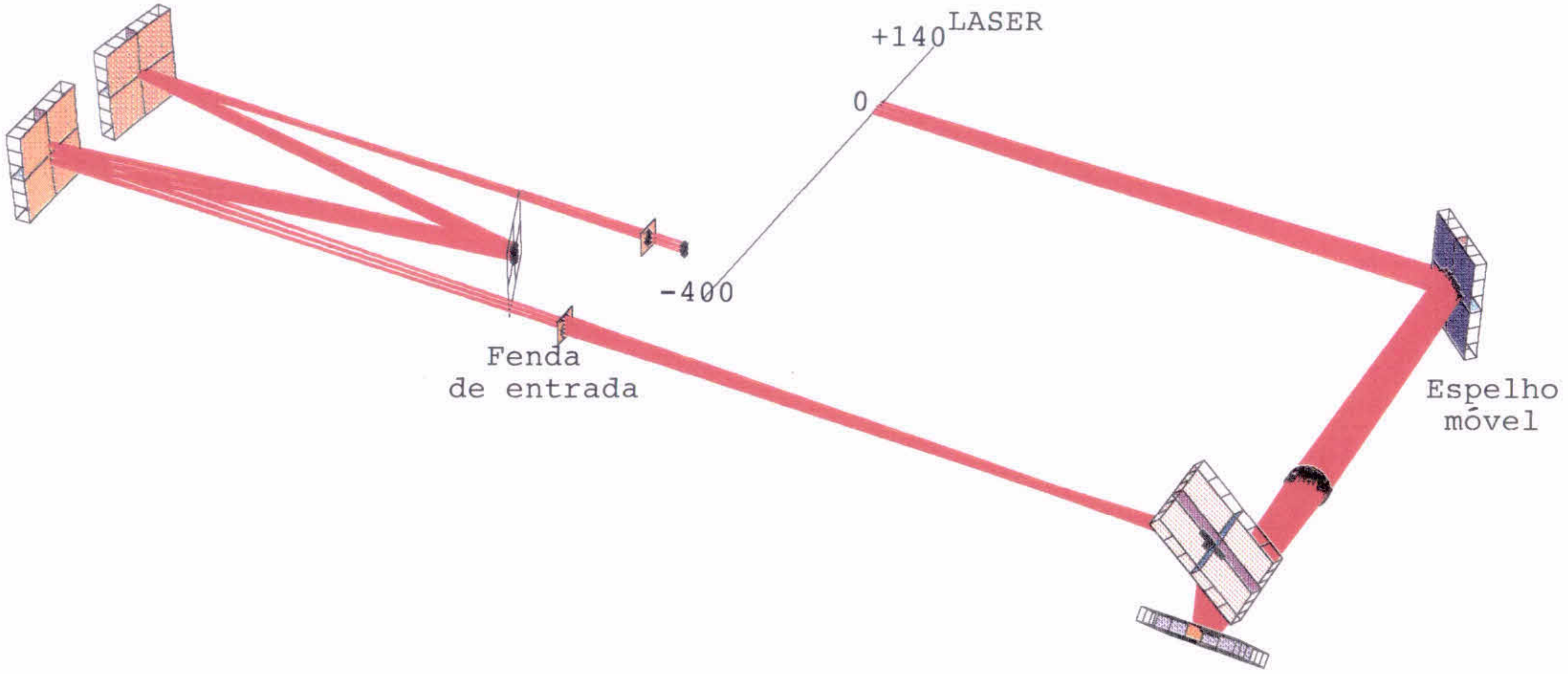

Figura 3.2 : Simulação do sistema de coleção por varredura.

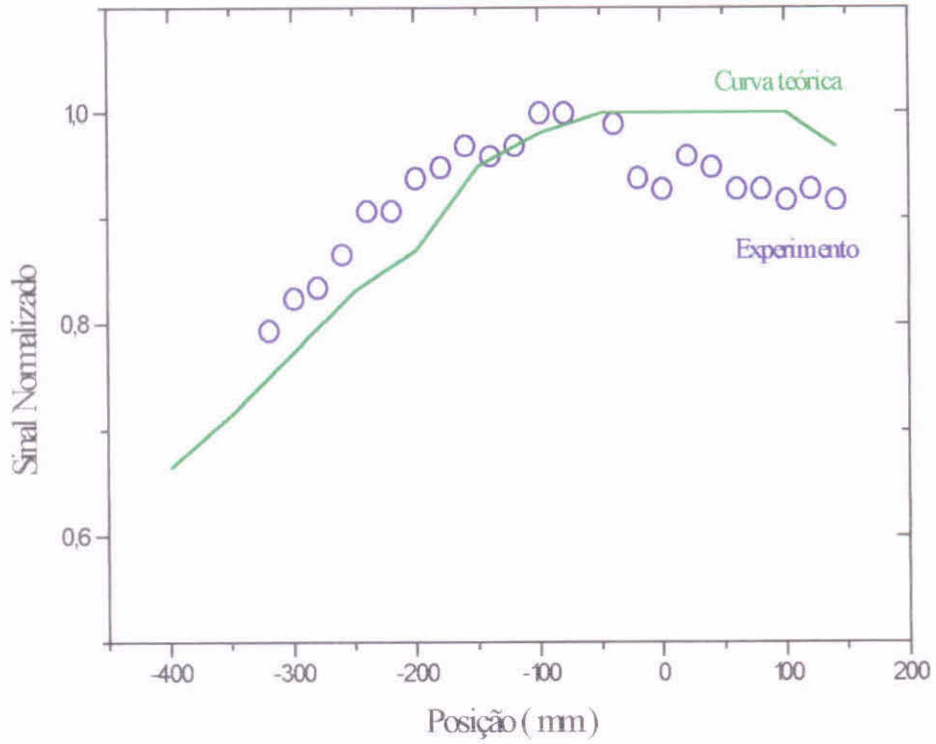

Figura 3.3 : Simulação e resultados experimentais com o protótipo do sistema de coleção por varredura

Capítulo 4

Espalhamento em Nitrogênio no Tokamak NOVA-UNICAMP

Durante o segundo semestre de 1997 acompanhei a instalação e os primeiros testes do sistema multipassagem de espalhamento Thomson implantado no tokamak NOVA-Unicamp.

Na figura 4.1 é apresentado um desenho esquemático do sistema implantado. Na figura 4.2 temos algumas curvas de espalhamento molecular com gás nitrogênio obtidas para diferentes números de passagens. Na figura 4.3 uma curva de amplificação em função do número de passagens é apresentada. Nesta curva podemos verificar um ganho máximo de 5 vezes sendo que o sistema satura para oito passagens. Duas conclusões importantes podem ser tiradas destes primeiros testes : 1) Tabalhar com um número de passagens superior a oito para o tokamak NOVA-Unicamp apenas contribui com um aumento do stray light sem apresentar um ganho justificavel ; 2) Para aumentar o ganho devem ser trocadas as janelas de entrada e saída da máquina, que são as principais responsáveis pelas perdas neste sistema.

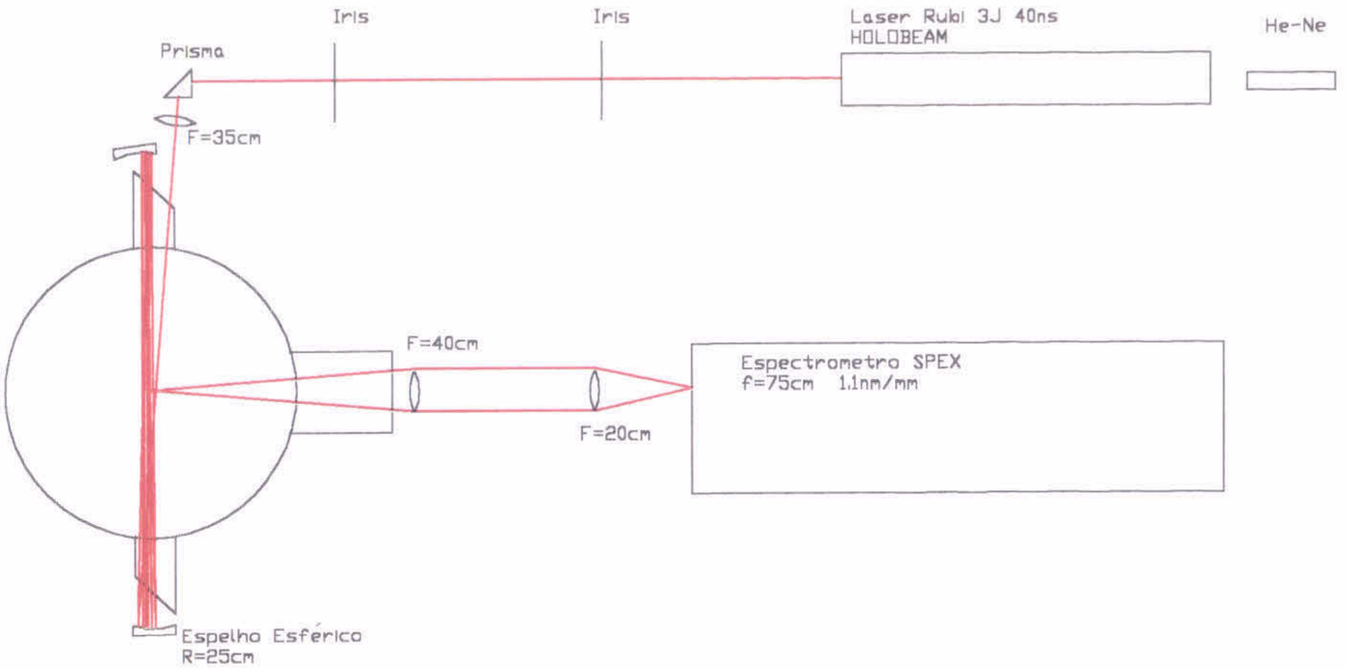

Figura 4.1 : Desenho esquemático do sistema de Espalhamento Thomson do tokamak NOVA-UNICAMP

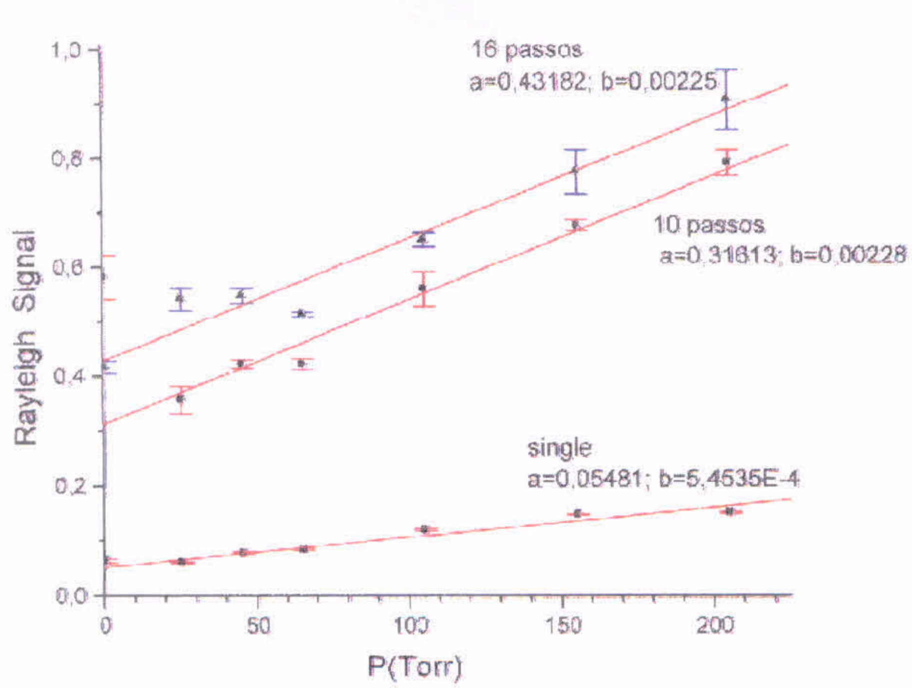

Figura 4.2 : Espalhamento Rayleigh multipassagem no tokamak NOVA.

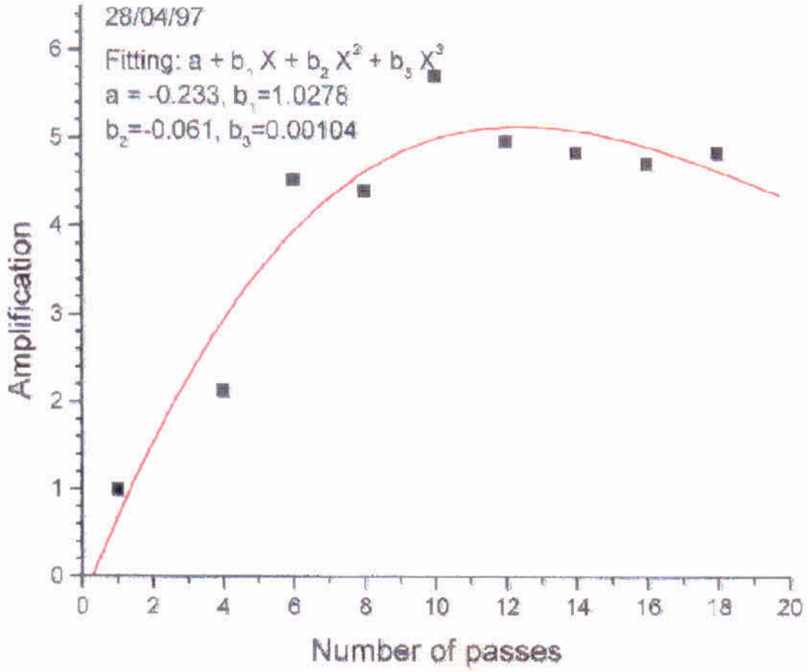

Figura 4.3 : Amplificação do sistema multipassagem.

Capítulo 5

Orçamento

Um levantamento completo dos custos para a implantação do diagnostico de espalhamento Thomson foi realizado durante o desenvolvimento do projeto. Na tabela 5.1 temos a especificação geral dos componentes e equipamentos necessários assim como o custo total do diagnóstico. Nas páginas seguintes são fornecidos os preços individuais de algumas partes. Devemos lembrar que o valor de R$ 393.000,00 representa um sistema completo e que versões mais simplificadas podem ser consideradas.

Quantidade	**Descrição**	**Valor R$**
1	Laser de rubi (10 J)	150.000,00
	Componentes e suportes óticos (MellesGriot)	53.000,00
3	Mesas óticas (MellesGriot)	17.000,00
1	Espectrômetro (Jobin Yvon - HR640)	40.000,00
2	Osciloscópios	30.000,00
7	Fotomultiplicadoras 9658R c/ 4 fontes	34.000,00
2	Fotomultiplicadoras XP1752	20.000,00
1	Lâmpada de calibração	6.000,00
3	Janelas para o ETE	10.000,00
	Módulo de aquisição	15.000,00
	Outros (computador, partes mecânicas, etc)	8.000,00
	Total	**393.000,00**

LUMONICS

Facsimile

To:	Luiz Angelo Berni - INPE/LAP - Brazil (00 55 12 325-6710)	Fax No:	0088
Copy To:		Pages:	5
From:	George Synowiec - Lumonics Ltd, Rugby	Date:	07 April 1997
Subject:	**Your Enquiry of 7 April 1997**		

Thank you for your fax enquiry. As requested please find attached a data sheet for the HLS range of ruby lasers.

Although these are specifically designed for holographic use, they are also the basis of the units we supply for Thomson scattering. The 10J/pulse model is the HLS4 This is available with double pulse operation at reduced energy. The double pulse separation range is variable between 1 and 800 microseconds. Budgetary Price for the HLS4-2 (ie 2 ppm) is GB£98,000, excluding delivery and installation, and excluding taxes. Delivery and installation costs would need to be confirmed, but could be up to approximately GB£12,000.

All our ruby lasers are now built to order and hence the delivery lead time is approximately 6 to 7 months.

Best Regards

H. E. Smith

pp

J A Synowiec
Marketing Manager - Low Power Lasers

RUGBY OPERATIONS

Lumonics Ltd
Cosford Lane, Swift Valley, Rugby
Warwickshire, CV21 1QN
England
Tel: (01788) 570321
Fax: (01788) 579824

conec

Proposta 401/97 São Paulo, 06 de Maiol de 1997

AO
INSTITUTO DE PESQUISAS ESPACIAIS (INPE/LAP)
Av. dos Astronautas, 1758
12201-970 - São José dos Campos - SP
At.: Sr. Luiz Ângelo Berni

Em atendimento a sua solicitação, apresentamos proposta para fornecimento de material produzido por nossa representada MELLES GRIOT:

ITEM	QTD.	MODELO	DESCRIÇÃO	UNIT.	TOTAL
1	1	09LBX005	Laser Beam Expander 20X	690.80	690.80
2	1	09LBV001	Zoom Beam Expander 2.5 x to 10x	1732.50	1732.50
3	1	07HBZ001	Zoom Beam Expander Mounting Stand	148.50	148.50
4	1	08WLB005/522	High Energy Laser Window	528.50	528.50
5	4	02MFG009	Mirror 10x10cm	244.20	976.80
6	2	02MFG013	Mirror 20x20 cm	1097.80	2195.60
7	2	02MFG013	Mirror 20x20 cm	1097.80	2195.60
8	2	01LPX337	Lens f=100cm - Ø=14.5cm	195.80	391.60
9	2	01LAO367	Lens f=100cm - Ø=15.0cm	2447.50	4895.00
10	3	03FSG017	Neutral Filter Set (7) - 50x50x2mm	311.30	933.90
11	2	03CFS007	Colored Glass Filter set (12)	652.30	1304.60
12	5	03FPG007	Polarizer	125.40	627.00
13	3	08MLB005/422	Mirror 45°	324.50	973.50
			LENTES DIVERSAS		
13	2	01LPX047	D=11.7 mm F-30mm	20.35	40.70
14	2	01LPX111	D=40 mm F-50mm	29.92	59.84
15	2	01LPX139	D=40 mm F-70mm	36.41	72.82
16	2	01LPX179	D=40 mm F-100mm	34.43	68.86
17	2	01LPX239	D=42 mm F-150mm	33.11	66.22
18	2	01LPX277	D=50 mm F-200mm	31.46	62.92
19	2	01LPX305	D=47 mm F-300mm	31.46	62.92
20	2	01LPX322	D=50 mm F-500mm	31.79	63.58
21	2	01LPX423	D=4.2 mm F-4mm	47.63	95.26
22	2	01LPX005	D=8 mm F-10mm	20.02	40.04
23	2	01LPX019	D=10 mm F-20mm	20.13	40.26
			PRISMAS		
24	3	01PRS029	A=B=C = 40mm	143.00	429.00
			ESPELHOS DIVERSOS		
25	2	02MFG001	25x25	18.92	37.84
26	2	02MFG005	50x50	20.24	40.48
27	2	02MFG007	75x75	22.99	45.98
			LASER		
28	3	05LHR111	Laser de HeNe 1mW	361.90	1085.70

conec comércio e importação ltda.
rua itapeva 486/490 - térreo
01332-902 - são paulo - brasil

fone: (011) 285 4755
fax: (011) 251 3832

ITEM	QTD.	MODELO	DESCRIÇÃO	UNIT.	TOTAL
29	1	05LHR171	Laser de HeNe7mW	841.50	841.50
30	3	05LPL911-065	Power Supply	277.20	831.60
31	1	05LPL903-070	Power Supply	357.50	357.50
			SUPORTES		
32	3	04IDC021	Iris Ø = 55mm	50.60	151.80
33	15	07LHA001	Adjustable Lens Holders Ø = 10-60	82.50	1237.50
34	5	07LHA004	Adjustable Lens Holders Ø = 5-25	77.00	385.00
35	2	07HVB003	V-Block Component Holder	108.90	217.80
36	5	07MMC001	Kinematic Mirror Mounts (50x50)	108.90	544.50
37	2	07MBM505	Precision Mirror Mounts Ø = 50	302.50	605.00
38	5	07DSM534	Stable Rod Mirror Mounts	522.60	2613.00
39	2	07MFM507	50mm Flexure Mirror Mount	247.50	495.00
40	2	07MAD005	Gimbal Mirror Mounts	731.50	1463.00
41	5	07HFU003	Filters Holders (50x50)	85.80	429.00
42	3	07TTM003	Post-Mounted Prism	137.50	412.50
43	2	07HPR005	Polarizer Holders	327.80	655.60
44	5	07HID003	Iris Diaphragm Holder	38.50	192.50
45	3	07HLH001	Cylindrical Laser Holders	247.50	742.50
46	30	07RMS001	Mounting Posts L=40 D=12 M6	11.00	330.00
47	30	07RMS003	Mounting Posts L=80 D=12 M6	13.20	396.00
48	20	07RMS005	Mounting Posts L=150 D=12 M6	15.40	308.00
49	5	07RML006	Mounting Posts L=40 D=20 M6	15.40	77.00
50	5	07RML009	Mounting Posts L=100 D=20 M6	18.70	93.50
51	5	07RML002	Mounting Posts L=150 D=20 M6	20.90	104.50
52	5	07RAD516	Thread Adaptors M6 - M4	18.70	93.50
53	5	07RAD513	Thread Adaptors M6 - M4	18.70	93.50
54	5	07RAD527	Thread Adaptors M6 - M16x1	20.90	104.50
55	15	07PHS511	Post Holders L=30 D=12	19.80	297.00
56	15	07PHS513	Post Holders L=50 D=12	23.10	346.50
57	5	07PHM503	Post Holders L=30 D= 8	28.60	143.00
58	5	07PHL513	Post Holders L=30 D=20	29.70	148.50
59	10	07CFL001	Post Clamps (right angle)	29.70	297.00
60	10	07CRL001	Post clamps (adjustable angle)	40.70	407.00
61	3	07DSC501	Post Carriers	85.80	257.40
62	10	07RPC506	Single-Slotted Mounting Bases	27.50	275.00
63	3	07BKS502	Kinematic Bases	236.50	709.50
64	10	07CTT501	Table Clamps L=50	12.10	121.00
65	10	07CTT502	Table Clamps L=72	15.40	154.00
66	3	07ORN003	Optical Rails h=50 L=0.5m	97.90	293.70
67	3	07ORN007	Optical Rails L=1.0m	189.20	567.60
68	15	07OCN503	Optical Rail Carriers l=65	79.20	1188.00

ITEM	QTD.	MODELO	DESCRIÇÃO	UNIT.	TOTAL
69	10	07TSC504	Steel Translation Stages L=65 (center drive)	302.50	3025.00
70	10	07TSS504	Steel Translation Stages L=65 (side drive)	302.50	3025.00
71	5	07TSB504	Angle Brackets	64.90	324.50
72	2	07TSZ504	Vertical Translation Stages	511.50	1023.00
73	2	07BLJ501	Lab Jacks	588.50	1177.00
74	3	07TRT501	Rotation Stages	412.50	1237.50
			MESA		
75	1	07OTR506	Optical Tabletop 1.5 x 5m e=21cm	7161.00	7161.00
76	1	07OTR534	Optical Tabletop 2.0 x 1.0 e=21cm	7366.00	7366.00
77	1	07OBC506	Optical Bredboard 0.6 x 0.9m	1246.00	1246.00
78	8	07OTL015	Rigid non-isolating support h=700mm	1045.00	8360.00
			TOTAL		72832.32

Fabricante:	MELLES GRIOT
País de Origem:	E.E.U.U.
Preços:	Posto FOB
Cond. de pagto.:	Carta de Crédito
Embarque:	4/6 semanas após recebimento dos documentos de importação
Garantia:	Um ano

Alcir Laerte Tanck Rocha

OBS.: Os preços acima sofrerão reajuste de 5%, devido a nova tabela do fabricante.

JOBIN YVON - SPEX
Groupe Instruments S.A.

~~ITA~~ INPE
Instituto Tecnologico da Aeronautica
Prof. Mario Ueda
Laboratorio de Plasma
BRAZIL

Our ref. :
LV-97-046EX

Longjumeau, 1997-September-1

QUOTATION

RÉFÉRENCE	DESCRIPTION	PRICE FRF.
21 311 000/MSL	**HR640 MSL** - Focal length 640 mm. - Aperture F/5.2 with 110 x 110 mm grating. - Aberration corrected Czerny-Turner design. - Interchangeable gratings (3 possible dimensions). - Spectral range : 190 nm - 40 µm (depending on the grating used). - Collimating mirror 110 x 110 mm. - Focusing mirror 110 x 140 mm. - Field at full aperture : 25 mm without aberration. - Includes stepper motor for Spectralink. - Supplied with a basic Spectralink controller, including : . PS - Rack mount kit (19") and power supply, . MDR - Motor Driver Module with joystick. - Possibility of axial and lateral slits, the latter with return mirror, controlled either manually or with a motor. - Possibility of axial exit adaptation for **1" multichannel detector**. - Minimum requirements : . Two slits, or one slit with a multichannel adapter, . One grating	139095
21 332 010/A1	Axial entrance slit, adjustable by micrometer screw	13717
21 338 010/C3	Axial adaptation for multichannel detector (JY type)	6281
530 27 160M	Blazed holographic grating - 1200 grooves/mm - 630 nm blaze - Spectral range 400-1300 nm	22572

ISO9002
Certificate No: 1005

ISO9002
Certificate No. 3971

Richardson Electronics, Ltd

Rua Inajaroba, 82
Sao Paulo SP, 04511-040 Brazil
Phone: +55-11-820-6199
Fax : +55-11-820-6199

Price Quotation 353742

08 DEC 1997 Page 1 of 1

Valid for 30 days

Customer 569675
Douglas Cavalli Giraldez
INPE INST PESQUISAS ESPACIAIS
AVENIDA DOS ASTRONAUTAS 1758
CP 515
S JOSE D CAMPOS SP 12227010
BRAZIL

Your Reference	Terms	Currency	Customer Fax
	Subject to approval	US Dollar	55213456710

Item	Qty	Part Number	Br	Unit Price	Extension	Delivery
1	1	XP1752/D1 PHOTOMULTIPLIER	PH	10,500.00	10,500.00	10 Weeks
2	1	FE4164 Socket for XP1752/D1	PH	250.00	250.00	10 Weeks
3	1	SPECIAL-ACCESRY VD107 ACCESSORIES		520.00	520.00	10 Weeks

All prices are FOB LaFox IL USA
Payment terms:Irrevocable and confirmed letter of credit at sight

Signed:
Enio Guedes

The Terms and Conditions of Sale of Richardson, a copy of which is on the back hereof, are agreed to and made a part hereof.

FIBERGUIDE INDUSTRIES

QUOTATION

To:	INPE/J.AP	May 12, 1997
Attn:	Luiz Angelo Berni	From: Jim Adamec
Phone:		Quote: JA0423721
Fax:	12-325-6710	

▶ Fiberguide Industries cannot offer a quotation for the coherent bundles. The production is out of our scope.

Description	Qty per shipment	Unit price
Fiber Optic Bundle 136 Fibers: APC210/230N Fiber area = 8 X 0.8mm Length = 10 meters P/N APBCB6582	1	$1856.00
Fiber Optic Bundle 136 Fibers: APC210/230N Fiber area = 8 X 0.8mm Length = 1.5 meters P/N APBCB6583	1	$929.00
Fiber Optic Bundle 860 Fibers: APC210/230N Fiber area = 8 X 2.0mm Length = 1.5 meters P/N APBCB6584	1	$2119.00

Current estimated shipment: 5wks ARO

TERMS & CONDITIONS:

- ▶ FOB Fiberguide, Caldwell, ID.
- ▶ Payment terms NET 30.
- ▶ Prices valid for 60 days.
- ▶ All orders are subject to credit approval before acceptance
- ▶ Minimum order: $500. Minimum line: $250.
- ▶ Maximum shipments / order: 5. For large quantities, different schedules may apply

Standard Estimated Shipment:

2-6 wks ARO, previously purchased items.

2-8 wks ARO, new items. An engineering drawing is faxed for approval 1-2 wks ARO. A delay in receiving approval may result in a delay of shipment. Design changes may affect the current prices.

After order is placed, Fiberguide can confirm shipment based on actual production commitments.

Jim Adamec
Sales Applications Engineer

1 Bay Street • Stirling, New Jersey 07980
908-647-6601 • Fax: 908-647-8464
http://www.fiberguide.com • e-mail service@sales_nj.fiberguide.com

Conclusões

Todo o projeto das partes mecânicas para o diagnóstico de espalhamento Thomson, assim como simulações, testes e um orçamento geral foram realizados nestes nove meses de trabalho (Abril/97 a Dezembro/97). Paralelamente foi especificado um sistema de limpeza por descarga glow para a câmara de vácuo do tokamak ETE, acompanhamento da implantação e testes do sistema multipassagem de espalhamento Thomson para o tokamak NOVA-Unicamp e início dos estudos para a especificação do sistema de interferometria do tokamak ETE. Em relação a máquina, continuei prestando ajuda na construção das bobinas poloidais que deve se estender ao longo deste primeiro semestre de 1998.

Em relação a ótica de coleção para o tokamak ETE verificamos que a lente coletora é o elemento mais importante quando se trata de um sistema multiposição de observação do plasma. Nas simulações realizadas com o programa OPTICA (Mathematica) observei grande influência da aberração esférica, coma , astigmatismo e curvatura de campo na formação das imagens quando se trabalha com imagens dentro e fora do eixo ótico. No caso de se utilizar fibras óticas para transportar os sinais da lente coletora até os espectrômetros, uma lente específica deve ser projetada para diminuir estas perdas principalmente pelo fato de se trabalhar com fibras de dimensões pequenas o que necessita uma boa focalização do sistema de coleção.

O primeiro sistema sujerido para o ETE é um sistema simples que utiliza espelhos e duas lentes coletoras. As duas lentes em contato é a maneira mais simples e barata de diminuir a aberração esférica. Neste sistema a imagem observada sempre está sobre o eixo ótico do sistema durante a rotação do espelho movél, o que diminui os problemas de formação da imagem. Porém neste sistema o maior problema é a desfocalização da imagem sobre a fenda de entrada do espectrômetro devido a variação da distância da fonte de luz. Nas simulações realizadas verificamos uma perda de até 40% neste sistema. Para o ETE é proposto a instalação deste sistema de espelhos ou um sistema de canal único com fibra ótica utilizando uma lente simples. Futuramente este sistema poderá ser modificado para multicanal acrescentando outras fibras e detetores e se for necessário substituir a lente coletora por outra mais adequada. Para detectar o espectro espalhado é proposto a utilização de 4 a 5 fotomultiplicadoras que posteriormente poderão ser substituidas por uma único detetor multicanal (XP1752).

O orçamento geral do sistema ficou aproximadamente em R$400.000,00 (ver cap. 5). Devemos observar que só o laser de rubi é responsável por R$150.000,00 e que com mais R$150.000,00 é possível implantar um sistema básico de espalhamento Thomson.

Apêndice A1

Programa : Sistema de Coleção por Varredura

```
Needs["Optica`Optica`"]


Clear[];
Clear[conetheta,conenum,angulo,thetaX,thetaY,desloc,
     fonte1,fonte2,fonte,lente1,lente2,espelho1,
     espelho2,espelho3,fenda,limites,sistema];

(*Numero de raios em cada cone de luz*)
conenum = 4;

(*Angulo maximo do cone*)
conetheta = 1.2;

(*Posição do espelho ao longo do feixe do laser
  a partir do angulo de 45*)
posicao = -50;

(*Posicionamento do espelho*)
angulo = ArcTan[posicao/690];
angulo =  180*angulo/Pi;

If[posicao==0,deltangulo=0];
If[posicao<0,deltangulo=-1*angulo/2];
If[posicao>0,deltangulo=-1*angulo/2];

thetaX = Cos[Pi*(45+deltangulo)/180]//N;
thetaY = Sin[Pi*(45+deltangulo)/180]//N;

(*Deslocamento e rotacao  da fonte de luz*)
(*Para cada grau de desloc. do espelho, corresponde
  a 2 graus de desloc. da fonte *)
desloc = -690*Tan[Pi*2*deltangulo/180]//N;
thetax = Cos[Pi*2*deltangulo/180]//N;
thetay = Sin[Pi*2*deltangulo/180]//N;

laser =  RectangleGraphic[{0,-400},{0,140}];
fonte1 = Table[ConeOfRays[j,NumberOfRays->conenum,
       WaveLength->0.6943],{j,0,conetheta,0.3}];
fonte2 = Table[Move3D[fonte1,{0,y,z},{thetax,thetay,0},
       0],{y,-10,10,5},{z,-1.5,1.5,3}];
fonte = Move3D[fonte2,{0,desloc,0},{1,0,0},0];
lente1 = Move3D[PlanoConvexLens[1080,45,3.5,
```

```
        CurvatureDirection->Back],{690,-376.5,0},
        {0,-1,0},0];
lente2 = Move3D[PlanoConvexLens[1000,45,3.5],
        {690,-380,0},{0,-1,0},0];
espelho1 = Move3D[Mirror[{101,126},14],{690,0,0},
         {thetaX,thetaY,0},0];
espelho2 = Move3D[Mirror[{101,126},14],{690,-630,0},
         {0,-1,-1},0];
espelho3 = Move3D[Mirror[{101,126},14],{690,-630,110},
         {1,0,1},0];


(*Monocromador*)
a = 80;
b= 90;
c = 108.22;
d1 = 530.01;
d2 = 530.01;
alpha1 = 1/2*ArcTan[a/d1]//N;
alpha2 = 1/2*ArcTan[b/d2]//N;
index = 1.000437077824583;
d = 1000/1200;

lambda = 0.6943;

m =1;
angles = FindRoot[{
        d*(Sin[thetam]-Sin[thetai])==m*lambda/index,
        thetai + thetam == 2*(alpha1 + alpha2)},
        {thetai,Pi/10},{thetam,Pi/10}];
theta = -180/Pi*((thetai/.angles[[1]]) - 2*alpha1)//N;

Clear[S1,S2];
S1 = PinHole[{30,30},{3,20}];
S2 = PinHole[{30,30},{3,20}];

Clear[M1,M2];
M1 = SphericalMirror[2*638.40,{110,110},15];
M2 = SphericalMirror[2*638.40,{110,110},15];

Clear[G];
G = GratingMirror[1200,{110,80},DiffractedOrders->{{1,1}}];

Clear[monocromador];
monocromador = Move3D[{
            Move[S1,{0,0,0}],
            Move[M1,{-c-d1,0,180+180/Pi*alpha1}],
            Move[G,{-c,a,180+theta},TwistAngle->180],
            Move[M2,{-c-d2,a+b,180-180/Pi*alpha2}],
            Move[S2,{0,a+b,0}],
            Boundary[{43,-90,-270},{-763,260,80}]},
```

```
            {-30,-630,110},{1,0,0},0];


limites = Boundary[2000];

sistema = DrawSystem[{fonte,laser,espelho1,lente1,lente2,
       espelho2,espelho3,monocromador},Boxed->False];
Clear[];
ShowSystem[sistema,PlotType->Surface,ShowRange->{6}];
Clear[];
ShowSystem[sistema,PlotType->TopView];
```

Apêndice A2
Fotomultiplicadora Multicanal

XP1700 family of multi-channel photomultipliers

The observation of low-light-level events distributed randomly in space and time is a field where the photomultiplier tube (PMT) remains unsurpassed. And when big detectors with high detection efficiency or fast response (or both) are essential, it has no equal. This is the case in nuclear and high-energy physics, cosmic ray experiments, and in X-ray, nuclear medicine and analytical instrumentation. In all these fields, there is, however, an increasing need for detection systems providing ever-higher spatial resolution. This usually means more detection channels, each with a smaller sensitive area – in other words, many very-small PMTs. Scaling down conventional PMTs, however, still provides only one detection channel, and miniaturization is limited by manufacturing technology to tube diameters of about 10 mm. For smaller detection channels, a PMT with a *spatial* response is required. Such technology is provided by the XP1700 multi-channel family. And when used with input-fibre multiplexing, these PMTs can reduce the cost of tracking low-occupancy events in high-energy physics experiments significantly.

The XP1700 PMT family currently comprises types with 64 or 96 channels, with a choice of glass or fibre-optic input window, the latter providing lower optical crosstalk. Unlike the XP4700 series which they succeed, all XP1700 PMTs are available potted with a machined ring for straightforward fastening and centring the PMT to an optical head (see photo, centre PMT).

TABLE 1 The XP1700 family

type number*	channels	input window	$sk_e(\lambda)$ at 400 nm (mA/W)	gain at 1150 V	dynode linearity, ≈5% (mA)	rise time (ns)
XP1702	64	clear glass	65	10^6	2	5
XP1722	64	fibre-optic	60			
XP1704	96	clear glass	65			
XP1724	96	fibre-optic	60			

The sides of the tubes are painted black;
this coating is not, however, guaranteed to be light-tight.
* potted versions with centring ring are available;
add suffix /A to type number, e.g. XP1702/A.

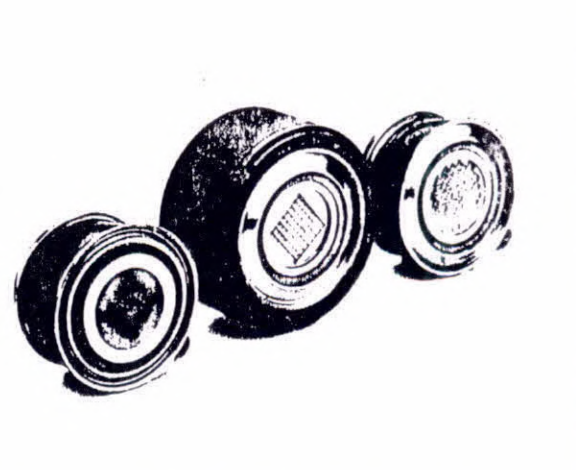

Available with 64 or 96-elements, the XP1700 family is a range of compact multi-channel PMTs with very low crosstalk. Illustrated are *(l to r)* the XP1722, XP1702/A (a potted PMT) and XP1704.

DESIGN AND OPERATING PRINCIPLE

All XP1700 family members have the same basic design, the main components of which, see Fig.1, are: a semi-transparent bialkali photocathode deposited on the input window, a compact metal-foil discrete-dynode electron multiplier, and a *segmented* output electrode providing up to 96 separate signal channels (Refs. 1 & 2).

Each XP1700 PMT provides low-crosstalk multi-channel light detection by photon to electron conversion, electron amplification and readout as in a conventional (single-channel) PMT. An XP1700 PMT is thus equivalent to an array of many miniature PMTs in one metal-sealed glass envelope.

The low inter-channel crosstalk results from the proprietary channel design shown in Fig.2 and which comprises:

- *proximity-focused input electron optics* which provides high spatial resolution and virtually no distortion. The two high-transparency grids can be used to optimize electron collection efficiency and to gate the tube (see *Tube gating*, p.10);
- *a discrete foil-dynode electron multiplier* which amplifies with very-low inter-channel crosstalk, owing to a patented design that minimizes electron dispersion between successive dynodes. Each dynode comprises two regularly-perforated metal sheets. One sheet is a field electrode, the other is the emissive electrode whose surface has a high secondary emission coefficient. A complete multiplier comprises a stack of several (usually nine) dynodes with aligned apertures;

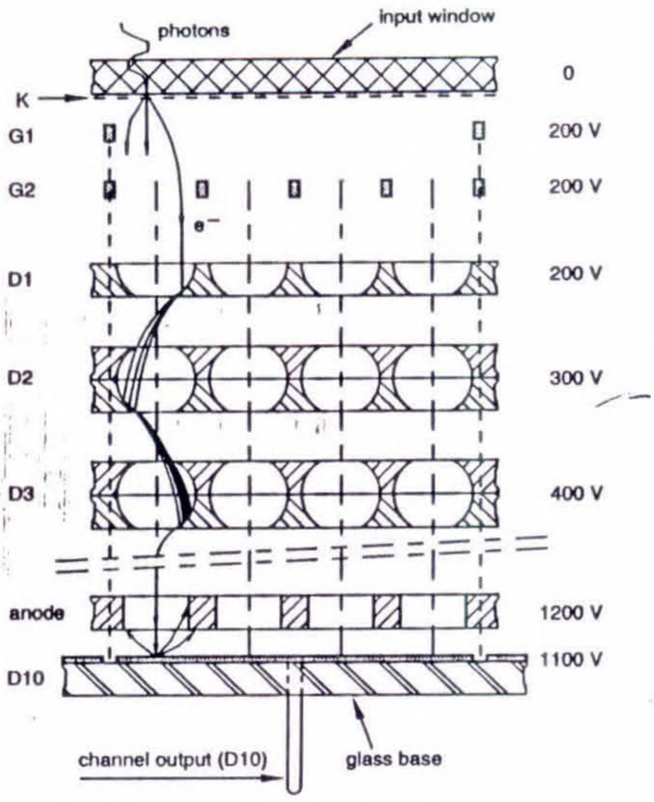

Fig.2 Cross-section through one detection channel. G1 and G2 are high-transparency grids; D1 to D10 dynodes, the latter segmented.

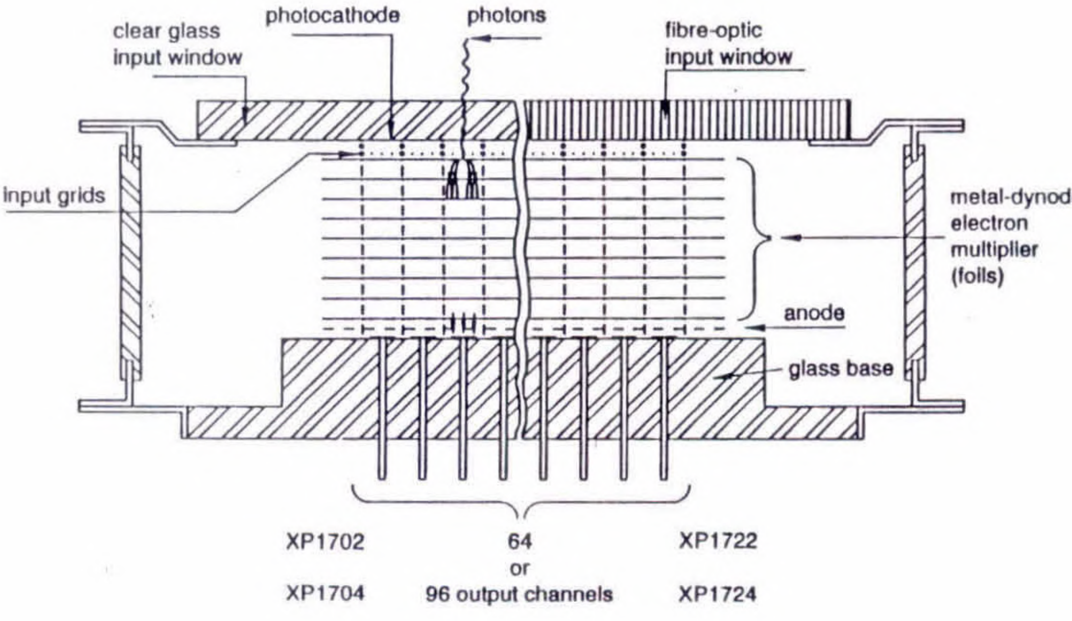

Fig.1 XP1700 PMT family construction (schematic).

14 = ?

- *an output section* which is very similar to that of a conventional PMT with a high-transparency anode grid between the last two dynodes. The last dynode, however, is segmented to form an array of 2.54 mm[*] square elements which provides imaging ability. Each element is electrically insulated from all others and forms one output channel. The anode is common to all channels.

SPATIAL RESOLUTION AND CROSSTALK

An XP1700 family PMT can detect and locate up to 64 or 96 low-light-level events simultaneously and without ambiguity. This is largely owing to the low crosstalk both in the input optics and through the electron multiplier. However, since all channels share a common photocathode, the way the photocathode is illuminated by the user can affect crosstalk slightly, and hence the ultimate resolution obtained.

Spatial resolution

Figure 3 shows the spatial resolution and crosstalk performance of an XP1700 family PMT. As this figure indicates, a channel is sensitive over the whole of its corresponding photocathode area (2.5 mm × 2.5 mm), and the crosstalk is low. The crosstalk is measured from the pedestal signal current (that part of the signal spreading from the illuminated pixel row to adjacent ones). As might be expected due to the multiplier design, illumination near to a pixel edge produces more inter-channel crosstalk than illumination near the pixel centre.

Optical crosstalk

Optical crosstalk can occur in the window as well as in the input electron optics. It depends on the optical coupling between the light event to be observed and each photocathode pixel (that area of the photocathode plane corresponding to one channel), and thus on the window type.

Parallel or focused pixel illumination

Inter-channel crosstalk is minimized in the case of parallel illumination, or focused illumination of the photocathode plane by a glass- or sapphire-sphere microlens, see Fig.4(a).

Direct illumination and illuminated pixel area

The percentage of a pixel that is illuminated has a small but measurable influence on crosstalk. Figure 5(a) shows the inter-channel crosstalk for direct illumination of a glass-window PMT (XP1702) and a fibre-optic window PMT (XP1722) for several collimated light beam diameters.

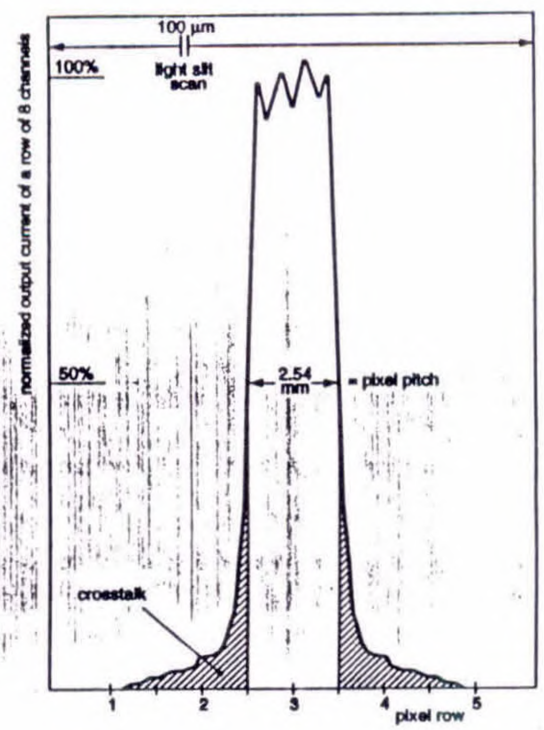

Fig.3 Spatial resolution and crosstalk scan. (Five pixel rows scanned, all measurements made on row 3). Light source: 100 µm slit, one pixel row long; scanning perpendicular to the pixel rows. Tube: XP1702.

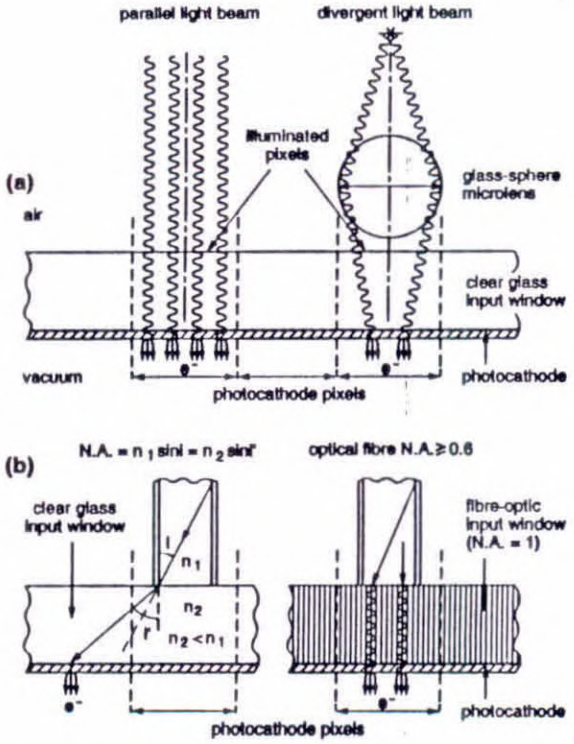

Fig.4 Photocathode illumination:
(a) direct, for a parallel and *(right)* a focused light beam.
(b) via an optical fibre onto a glass window and *(right)* onto a fibre-optic window (contact coupling).

---

[*] For convenience, the size of the elements is hereafter referred to as being 2.5 mm square.

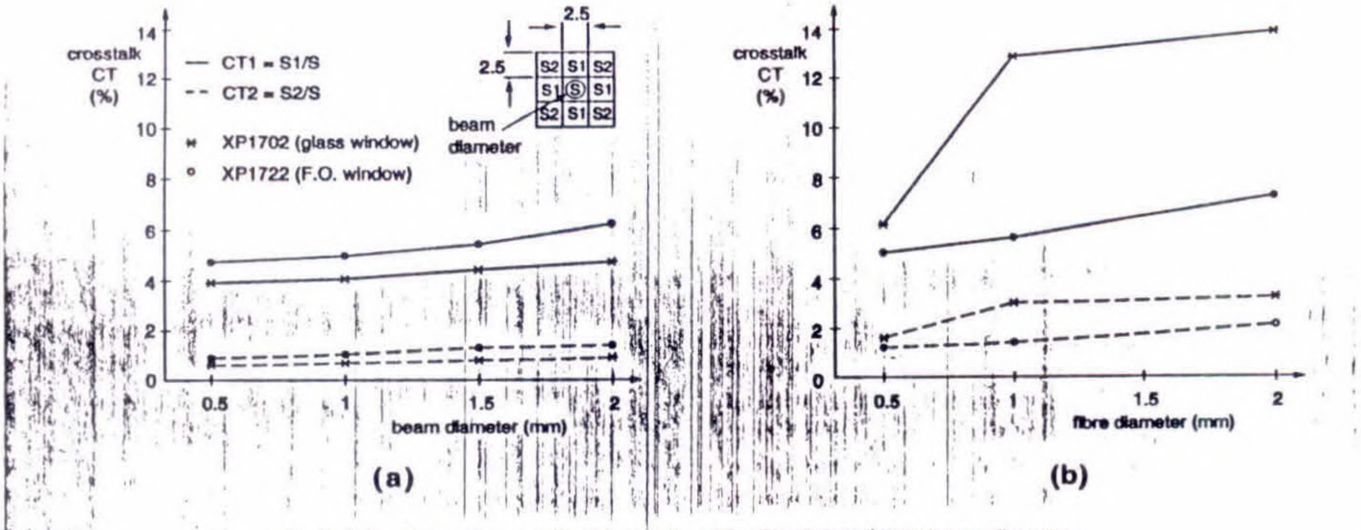

Fig.5 Inter-channel crosstalk: (a) as a function of collimated light beam diameter; (b) as a function of optical fibre diameter (contact coupling).

The measurements for the XP1702 are in accordance with those of Fig.3. Crosstalk (CT1) in each of the four pixels (S1 pixels) nearest to the illuminated one (S) is less than 5% for a 2 mm diameter light beam (about 50% pixel area illumination) centred on pixel S. For the XP1722, the slightly higher crosstalk is due to the higher optical crosstalk in the input electron optics caused by the numerical aperture of the window fibres.

As might be expected, the crosstalk (CT2) in the four corner pixels (S2 pixels) is much lower than for the touching pixels (about a fifth of CT1), and is <1% up to a beam diameter of 2 mm. This indicates a unique feature of an XP1700 PMT – crosstalk of <1% by operating a tube with a staggered channel arrangement. For example, by operating 32 of the 64 channels of an XP1702 or XP1722, or 48 of the 96 channels of an XP1704 or XP1724, see the

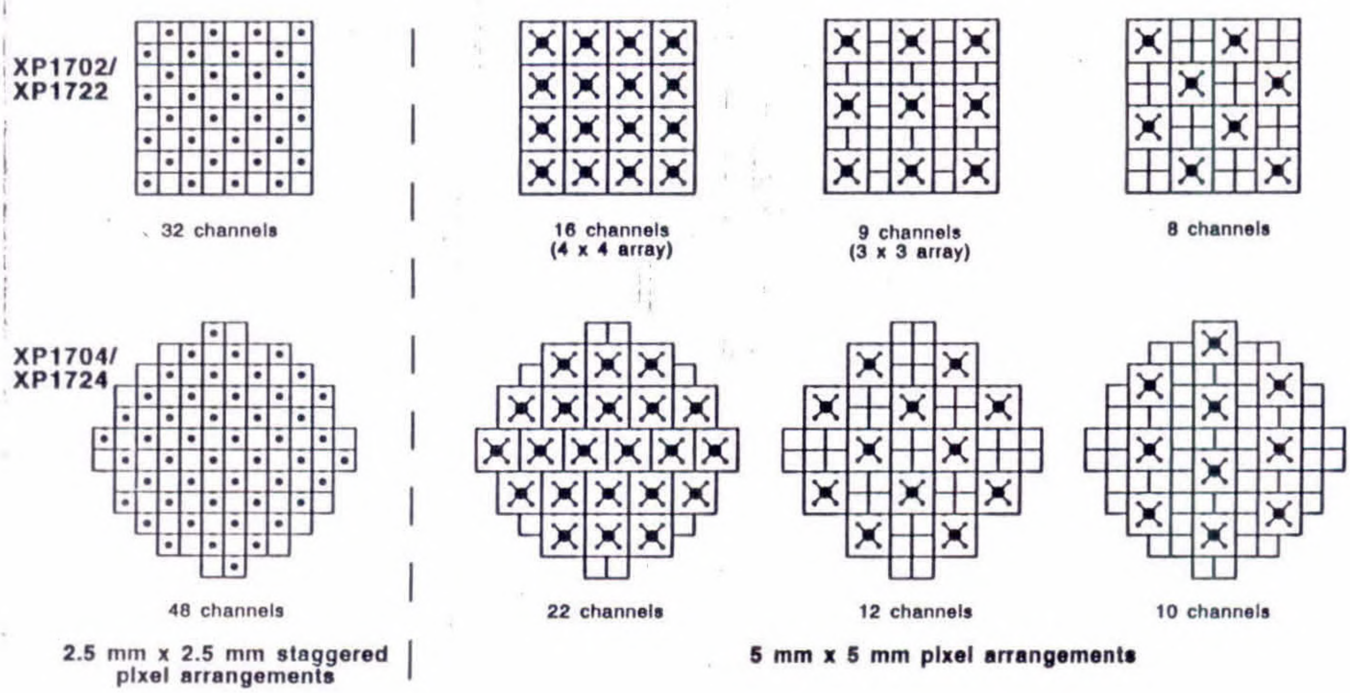

Fig.6 Some output channel arrangements for very low crosstalk. In the 9 and 10-channel arrangements, the unused channels can be connected to form a surrounding 'guard' electrode.

left part of Fig.6

Another possibility (also shown in Fig.6) to accommodate larger illuminated areas, or when lower crosstalk is required, is to connect four adjacent channels together to form one larger one of 5 mm square. This is done by interconnecting several of the segmented-dynode D10 pins. The CT1 crosstalk between the enlarged channels then decreases to <2% (for 2 mm light beam illumination), and for a staggered channel arrangement, to <0.3%, see Table 2.

TABLE 2 Crosstalk for several enlarged (5 mm × 5 mm) pixel arrangements

pixel arrangement, see Fig.6	crosstalk*	
	CT1 type	CT2 type
16 channels	1) ≤2% 2) ≤3%	1) ≤0.3% 2) ≤0.6%
9 channels with guard electrode	1) ≤0.2% 2) ≤0.4%	1) ≤0.04% 2) ≤0.07%
8 channels, staggered	negligible	1) ≤0.3% 2) ≤0.6%

* Two crosstalk values are given for illumination:
1) by a ϕ2 mm light beam, and 2) by a ϕ2 mm optical fibre.
All values are measured for an XP1702, but are also valid for an XP1704 where the pixel arrangement is identical.

Illumination by optical fibre

In an increasing number of particle detectors, light is conveyed to the PMTs through a glass or plastic optical fibre. In some detectors, the fibre itself is scintillating for detecting and localizing charged particles, X-rays or gamma rays. Fibre diameters range from about 2 mm down to some 50 μm.

As Fig.5(b) shows, coupling an optical fibre onto a glass-window PMT causes a relatively large optical cross-talk in the window due to the fibre's numerical aperture (usually >0.6), and to the thickness of the window (the minimum thickness being limited by vacuum considerations). As an example, a 1 mm diameter optical fibre coupled to a 3 mm thick glass window gives a cross-talk of ≈13% compared with 4% for illumination by a collimated light source of the same diameter (see Fig.5). If the fibre diameter is small enough (<500 μm), the use of a microlens array is a good way of reducing crosstalk, as already described. Alternatively, the use of larger pixels can lower crosstalk significantly, even with a 2 mm diameter fibre.

When slightly lower sensitivity can be tolerated, an XP1700 tube with fibre-optic window will improve cross-talk performance. As Fig.4(b) shows, light scattering in the window is virtually eliminated, and crosstalk is only about 5% with a 1 mm optical fibre (Fig.5(b)), and for a staggered pixel arrangement, less than 1.5%, making the XP1722 and XP1724 highly attractive in detection systems with optical-fibre readout.

Figures 7 to 10 show additional independent measurements of crosstalk and the dynode response of 64 and 96-channel tubes.

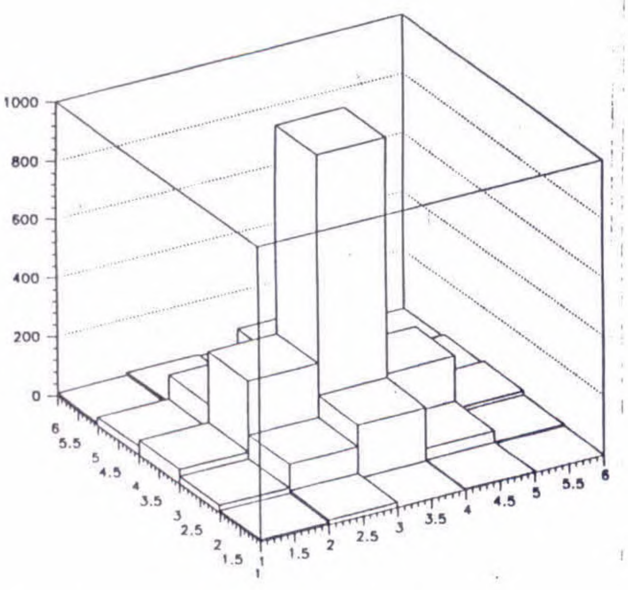

Fig.7 Inter-channel crosstalk of an XP1704 (25 channels only). One pixel illuminated by a 1 mm dia. input fibre centred on the pixel. Vertical axis: signal amplitude, arbitrary units; horizontal axes: 0.1" units (i.e. one pixel width). The crosstalk is largely optical crosstalk due to the XP1704's *glass* window.
Source: UCLA, USA.

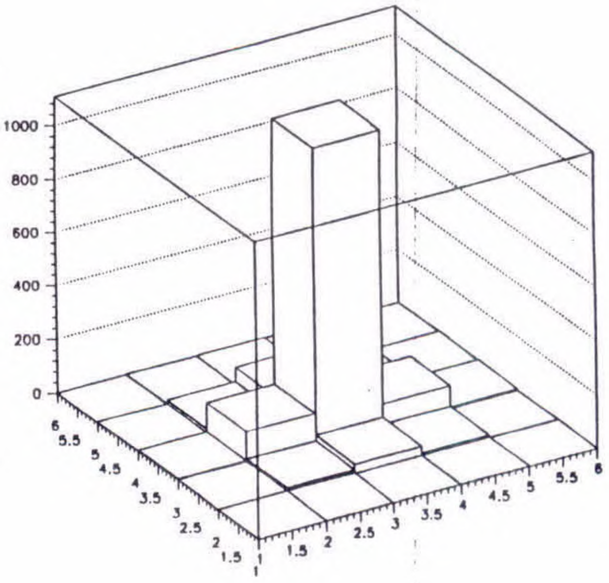

Fig.8 Inter-channel crosstalk of an XP1724 (25 channels only). Measuring conditions and axes as for Fig.7. Note the reduced crosstalk compared with that shown in Fig.7 owing to the XP1724's *fibre-optic* window.

Source: UCLA, USA.

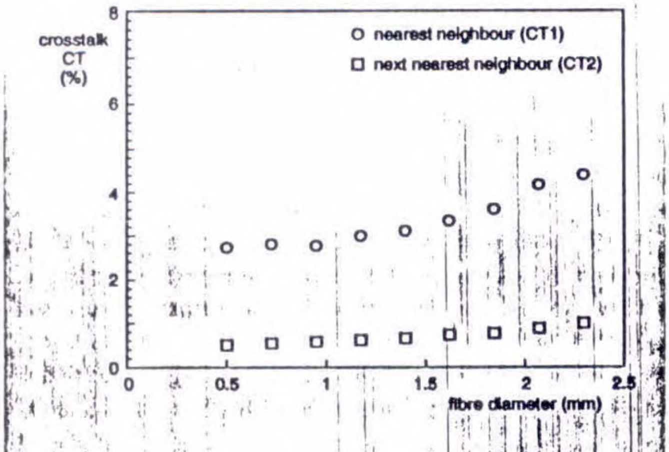

Fig.9 Inter-channel crosstalk of an XP4722 (XP1722 predecessor) as a function of input fibre diameter with the fibre accurately centred on one pixel.

Source: Yale University, USA.

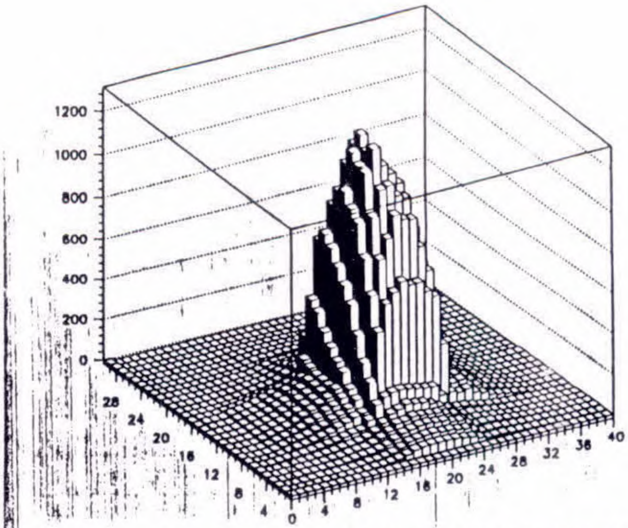

Fig.10 Dynode response map of one channel of an XP4722 scanned by a 500 µm fibre, with overscanning into adjacent channels. All values were measured at the channel dynode, but are plotted at the corresponding fibre locations. Vertical axis: relative signal amplitude, arbitrary units. Horizontal axes: mapping steps of 0.01" (0.25 mm, or ≈10 steps/channel).

Source: Yale University, USA.

INTER-CHANNEL UNIFORMITY

There is always some very small variation in the anode sensitivity of a conventional (single-channel) PMT when a light spot is scanned over the photocathode. This variation comes mainly from small spatial non-uniformities in the photocathode response, and in the collection efficiency of the first multiplier stage. In a multi-channel XP1700 PMT, the dynode output sensitivity spread between channels is mainly due to local variation(s) of gain at each multiplication stage, and to a lesser extent from the non-uniformities of a single-channel PMT just mentioned.

The inter-channel gain uniformity is usually measured by operating a PMT at typical gain with the signals from all pixel channels summed, then illuminating each photocathode pixel in turn with a light spot of ≤2 mm diameter, and measuring the variation in output signal. Another method is to uniformly illuminate the whole of the useful area of the photocathode and measure the individual

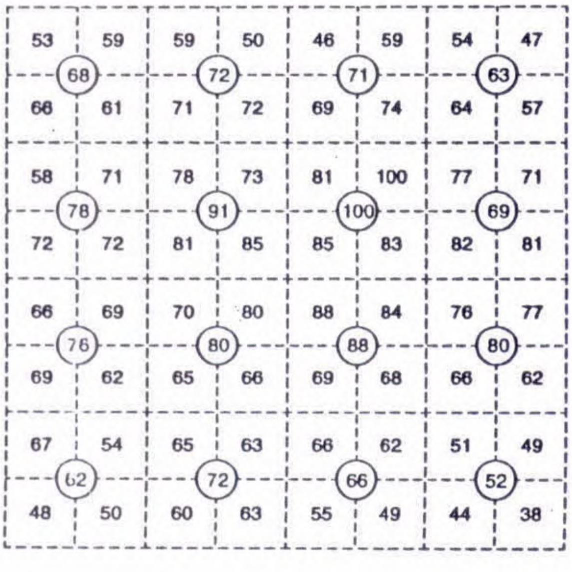

53	59	59	50	46	59	54	47
66	61	71	72	69	74	64	57
58	71	78	73	81	100	77	71
72	72	81	85	85	83	82	81
66	69	70	80	88	84	76	77
69	62	65	66	69	68	66	62
67	54	65	63	66	62	51	49
48	50	60	63	55	49	44	38

(68)	(72)	(71)	(63)
(78)	(91)	(100)	(69)
(76)	(80)	(88)	(80)
(62)	(72)	(66)	(52)

Fig.11 Normalized channel gain uniformity of an XP1702 for sixty-four 2.5 mm square pixels, and (circled numbers) for sixteen 5 mm square pixels. Values are normalized to the channel with the highest sensitivity, denoted by 100.

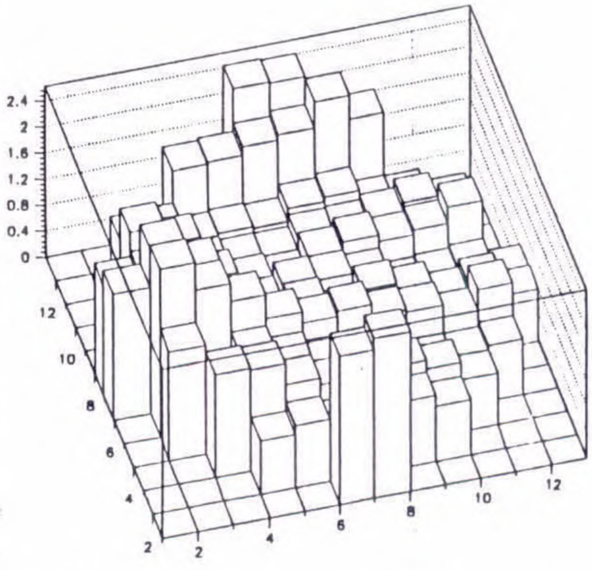

Fig.12 Dynode response map of the 96-channels of an XP1724. Each pixel illuminated in succession by a 1 mm dia. input fibre centred on each pixel. Vertical axis: relative signal amplitude, arbitrary scale. Horizontal axes: 0.1" units.

Source: UCLA, USA.

output channel currents.

Inter-channel gain uniformity is specified as the ratio between the maximum and the minimum channel output sensitivities. This ratio is approximately 3:1 over all of the 2.5 mm square pixels, see Fig.11, while the sensitivities of any two adjacent channels are within 30% of each other.

As might be expected, when several channels are connected together to form enlarged arrays, uniformity improves.

Fig.12 shows the results of independent measurements for an XP1724.

SINGLE AND MULTI-ELECTRON PULSE DETECTION

The single photoelectron detection performance of a PMT is given by the shape of the signal amplitude distribution (spectrum). The width of the single-electron peak in this spectrum is referred to as the pulse height resolution, PHR*, and depends on the relative variance of multiplier gain, that is, on the secondary emission properties and collection efficiencies of the first two multiplier stages.

The single-electron spectra of the XP1700 PMT family show a distinguishable, but not well-defined peak (PHR 150% to 200%) owing to the moderate gain of the first multiplier stage, but this is still adequate to allow very-low-light-level events to be detected. The PHR characteristics can vary from channel-to-channel due to local variations of the secondary emission of the first dynode.

The PHR of a multi-electron spectrum (e.g. scintillation detection) is mainly related to photocathode sensitivity, input collection efficiency and, to a much lesser extent, variations in multiplier gain. The typical channel PHR of an XP1700 family PMT is 80% to 90% for a ten-photoelectron input pulse. The PHR does not differ significantly between channels; any difference originating mainly from small differences in photocathode pixel sensitivity.

References 2 to 6 provide additional reading on this subject.

PULSE LINEARITY

The channel dynode linearity of a multi-channel PMT is relatively low compared with that of a conventional PMT – about 2 mA (5%) to 5 mA (10%), as measured by Yale University and UCLA. This is illustrated in Figs.13(a) and (b) for 1400 V and 1000 V supply voltages respectively. Dynode pulse saturation occurs in both cases at about 100 pC. With 1000 V supply voltage, the PMT was operated at a dynode gain of 7×10^4, so a single electron represents 0.0112 pC, and the electronic threshold in this arrangement was 0.1 pC (10 photoelectrons), resulting in a useful linear dynamic range of 1000:1, limited at the low end mainly by the measuring preamplifier. When the light levels to be detected allow the tube to be operated at a lower gain, a higher dynamic range results.

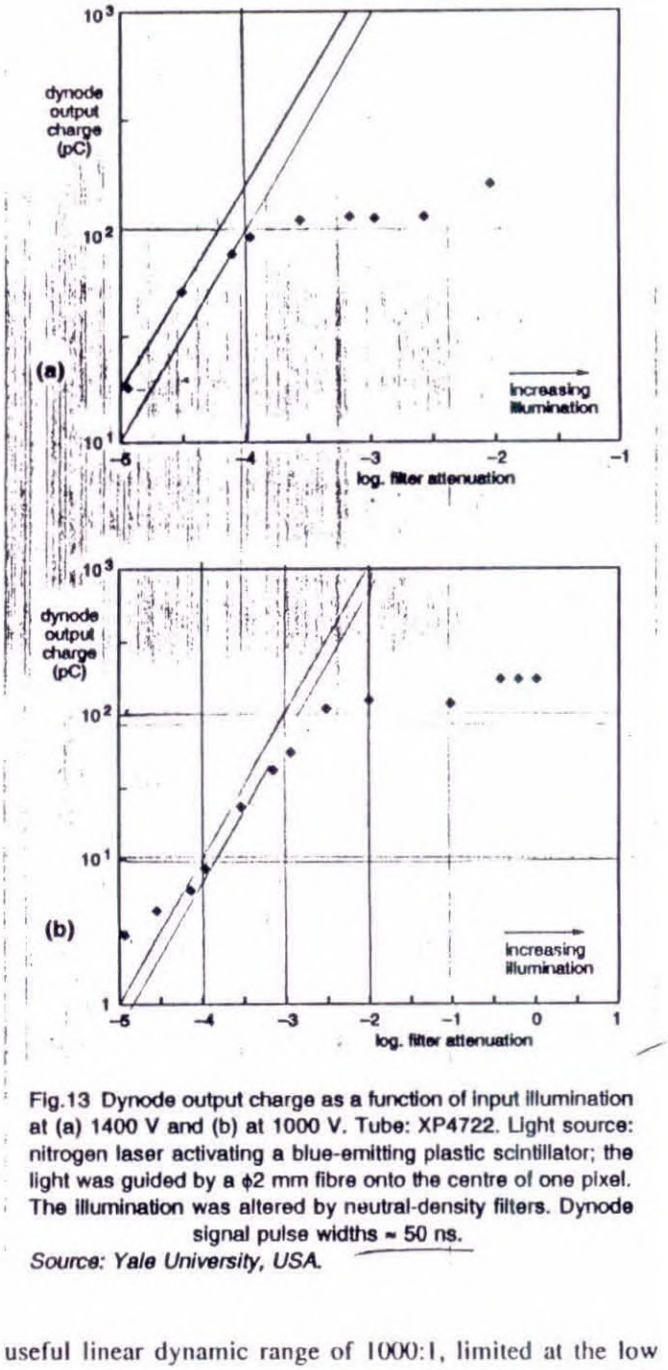

Fig.13 Dynode output charge as a function of input illumination at (a) 1400 V and (b) at 1000 V. Tube: XP4722. Light source: nitrogen laser activating a blue-emitting plastic scintillator; the light was guided by a ϕ2 mm fibre onto the centre of one pixel. The illumination was altered by neutral-density filters. Dynode signal pulse widths ≈ 50 ns.

Source: Yale University, USA.

IMMUNITY TO MAGNETIC FIELDS

Although not specifically designed to operate in strong magnetic fields, proximity-focused input electron optics and foil dynodes make the XP1700 family much less sensitive to magnetic fields than conventional PMTs.

Figure 14 shows the effect of an axial magnetic field on the gain of an XP1700 PMT and that of a conventional PMT. The XP1700 response is flat over all channels up to about 100 gauss, then falls rapidly (halving by 130 gauss). The gain reduction is caused by the effect of the field on

---

* strictly, $\mathrm{PHR} = \frac{\mathrm{FWHM}}{\mathrm{peak}} \times 100\%$ defined at a given photon illumination, FWHM being the full-width half-maximum.

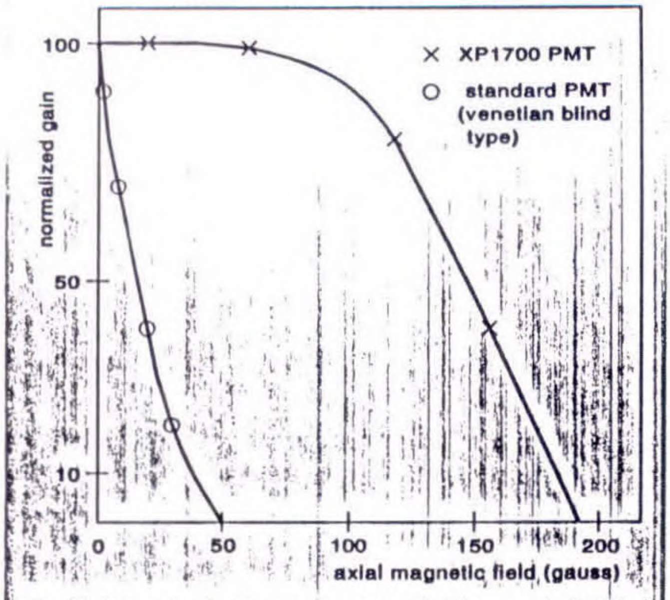

Fig.14 Normalized gain as a function of axial magnetic field for a conventional PMT and an XP1700 multi-channel PMT

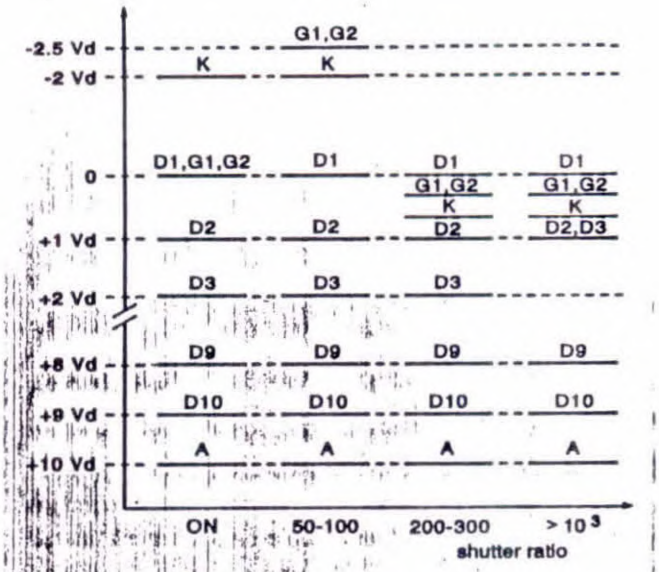

Fig.15 Relative multiplier voltage distributions for different shutter ratios.

the multiplier and not by the input optics whose proximity design makes this stage virtually insensitive to axial magnetic fields. In fact, this design has a beneficial influence on the overall crosstalk – lowering it, in an axial magnetic field, but at the expense of reduced gain (a 20% improvement in crosstalk corresponding roughly to a halving of gain). For a conventional PMT, an axial field of only a few gauss is sufficient to cause a large drop in gain, even when illumination is limited to the centre of the photocathode.

References 6 and 7 provide additional reading on this subject.

TUBE GATING

As already mentioned, the proximity-focused input optics of the XP1700 family has a pair of flat high-transparency grids between the photocathode (K), and the first dynode (D1) which has the same sensitive area as the photocathode, see Fig.2. The most efficient way to reduce the sensitivity of the tube without changing the voltage applied to the multiplier (between D1 and the anode) is to prevent photoelectrons from leaving the photocathode, and any photoelectons leaving D1 from reaching D2 (note, D1 behaves as an opaque photocathode for those photons that pass through the semitransparent one). This can be done by setting the potentials of the photocathode and grids G1 and G2 slightly positive with respect to the potential of D1. Two simultaneous voltage pulses are needed (one on G1 and G2, the other on the photocathode). Using this arrangement, the sensitivity of a tube can be reduced by more than a factor of 100 (shutter ratio). A lower shutter ratio (50 to 100) can be obtained more easily, simply by setting the potential of the grids negative with respect to the photocathode.

For higher shutter ratios, it is also necessary to modify the inter-electrode voltages of the multiplier. For example, making the potential of D3 the same as that of D2, (without altering the total multiplier voltage) produces a shutter ratio of about 1000.

Figure 15 summarizes the relative voltage distributions required for these different shutter ratios.

SIGNAL PROCESSING

Parallel processing

Owing to its negligible inter-channel crosstalk, an XP1700 family PMT can be considered equivalent to 64 or 96 PMTs. Parallel processing of all 64 or 96 light channels provides positional information, as well as relative amplitudes and timing.

The common anode signal which carries the sum of the channel output signals can also be used for amplitude analysis or as a trigger for other equipment.

Semi-parallel processing

Sixty-four or 96 discrete events can be resolved using considerably fewer processing channels, thus saving processing overhead, by connecting the output pins of one row to a distributed transmission line (resistive, RC or LC), and obtaining the position of the excited pixel(s) in the row by one of three standard methods (Refs. 2 and 8):

- charge division method
- rise time method
- delay line method.

Charge division method (for a resistive line)

If the charges collected at the ends of the transmission line are Q_A and Q_B, see Fig.16, the position (i) in the row of

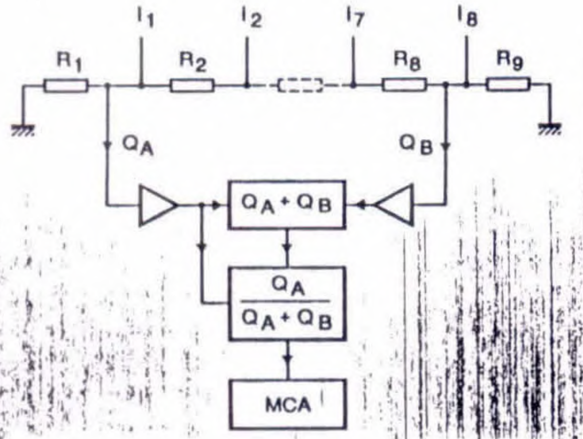

Fig.16 Measuring circuit for the charge division method.

the pixel excited at the input is given by the ratio of the charges:

$$\frac{Q_A}{Q_A+Q_B} = \frac{i}{8}$$

where i = 1 to 8 (for a 64-channel tube).

Rise time method (for an RC line)

Here, the positional information is derived from rise time measurements of the pulse(s) at one end of the line, the pulse shape depending on which pixel(s) are illuminated.

Delay line method (for an LC line)

The positional information is derived directly from the difference in transit time of the signals, measured at each end of the delay line.

X-Y localization

Localization of light events with a spatial resolution better than the pixel pitch can be obtained by allowing the light to fall on adjacent photocathode pixels (i.e. multi-photon light events) and processing the signals to calculate the centroid of the electron-cloud distribution over the activated channels. Note that deliberately increasing the crosstalk (by adjusting the G1 and G2 potentials away from optimum values) can improve the localization of the centroid, owing to the increased number of statistical samples obtained. However, this will be accompanied by a dramatic reduction in the number of simultaneous events that can be handled.

MULTI-CHANNEL PMTS IN TELESCOPE DETECTORS

Reflecting telescopes with arrays of PMTs in the focal plane of the mirror are now being used (as an alternative to slow image-intensifier techniques) to observe fast Cherenkov light phenomena in the atmosphere produced by high-energy cosmic radiation. An array of discrete PMTs, however, loses information owing to the "dead" area between individual tubes mainly caused by the tube walls. With its 96 channels forming an almost circular small array, and with no dead area between channels, the XP1704 is well-suited to replace conventional PMT arrays in telescopes with mirrors of moderate size (say 50 cm diameter and 60 cm focal length). In such telescopes, the XP1704's 2.5 mm square pixel size provides a field of view of about 3° and an angular resolution of about 0.2°, see Figs. 17 and 18, and Ref.9.

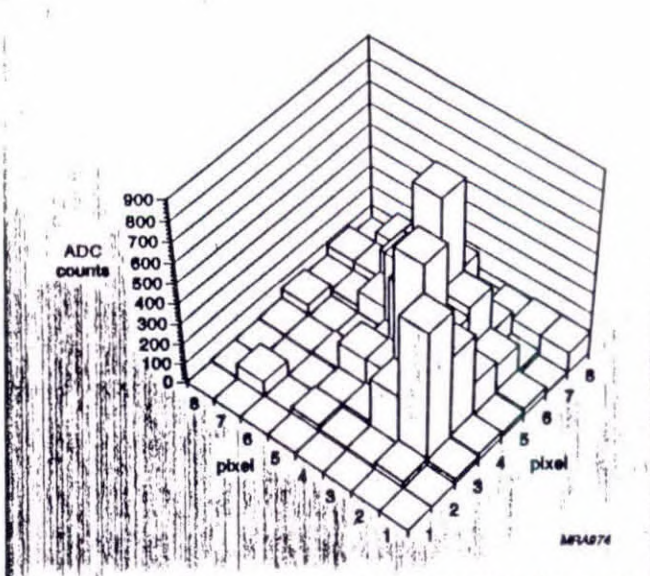

Fig.17 Image of Cherenkov light from an extensive air shower. Five ADC counts correspond to approximately one photo-electron. Values corrected for channel gain differences and ADC pedestals. Measurements were taken at the Astronomical Observatory of Campo Imperatore (EAS-TOP experiment, INFN National Gran Sasso Laboratories) using a 90 cm mirror with 64 cm focal length. PMT: XP4702; pixel angular resolution: 0.22°.
Source: INFN-CNR, Turin, Italy.

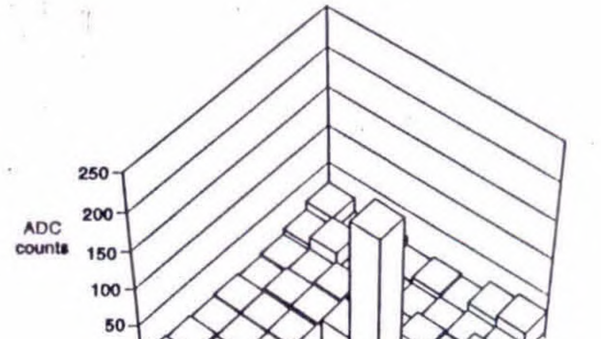

Fig.18 Image of the star ξ-Aquilae made using the same PMT telescope detector described in Fig.17 to calibrate the resolution of the telescope.
Source: INFN-CNR, Turin, Italy.

DIMENSIONS, PINNING AND ACCESSORIES

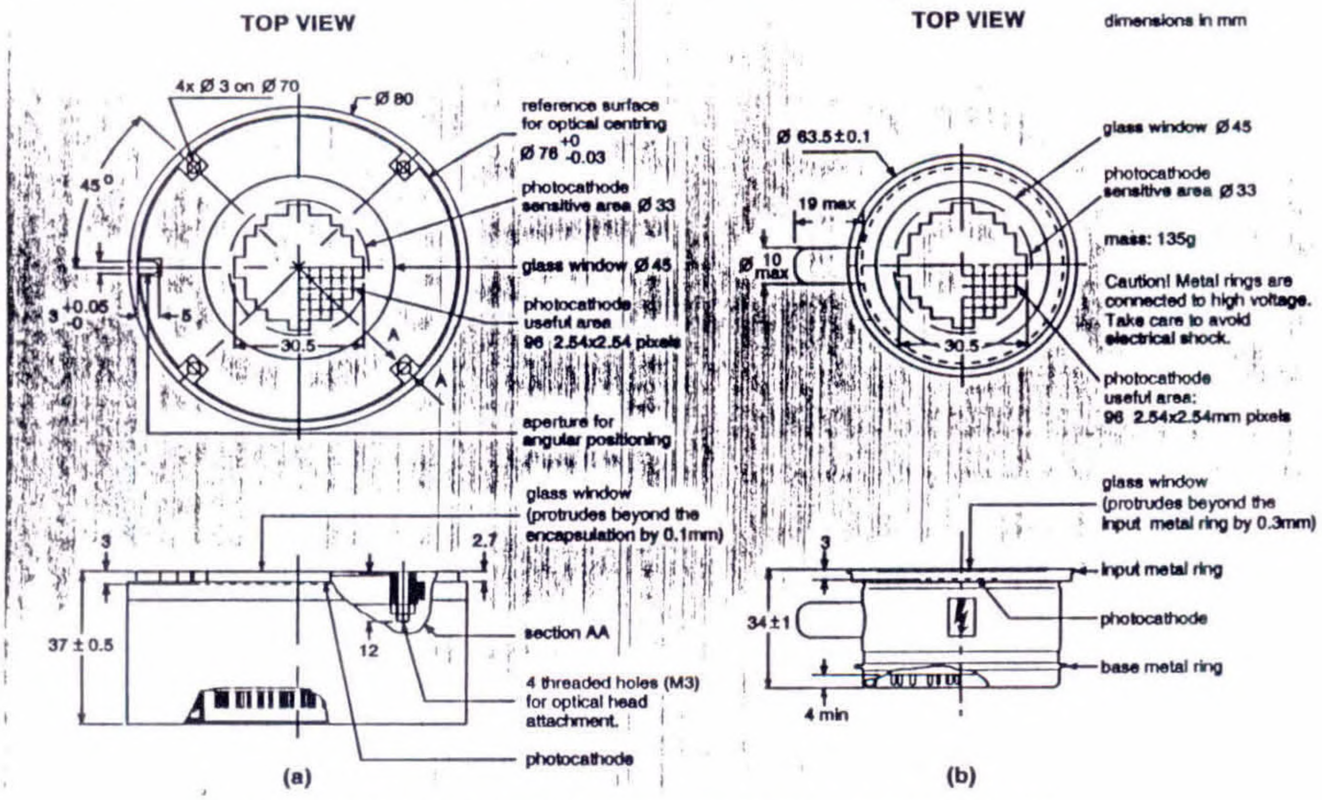

Fig. 19 (a) 96-channel potted PMT (XP1704/A) with centring ring and (b) naked version (XP1704). The 64-channel versions have an identical outline.

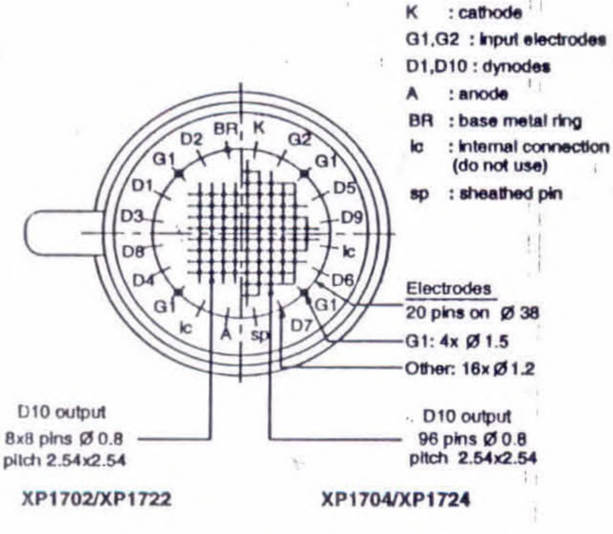

Fig.20 XP1700 family pinning.

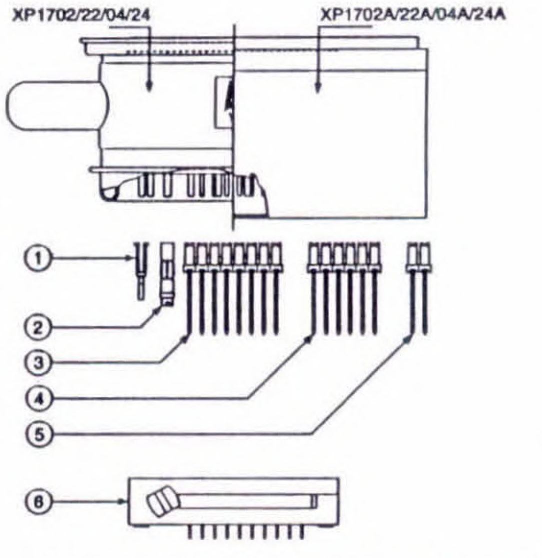

ref:	description	quantity		
		XP1704/24	XP1702/22	
1	pin connectors for all electrodes except G1 and D10	12	12	supplied with the tube
2	pin connector for G1	1	1	
3	8-pin extension strips for D10	8	8	
4	6-pin extension strips for D10	4	n.a.	
5	2-pin extension strips for D10	4	n.a.	
6	grid zip socket	1*	1**	

* 13x13 grid, ordering code FE4196

** 10x10 grid, ordering code FE4184

Fig. 21 XP1700 family pin connectors and zero-insertion-pressure socket.

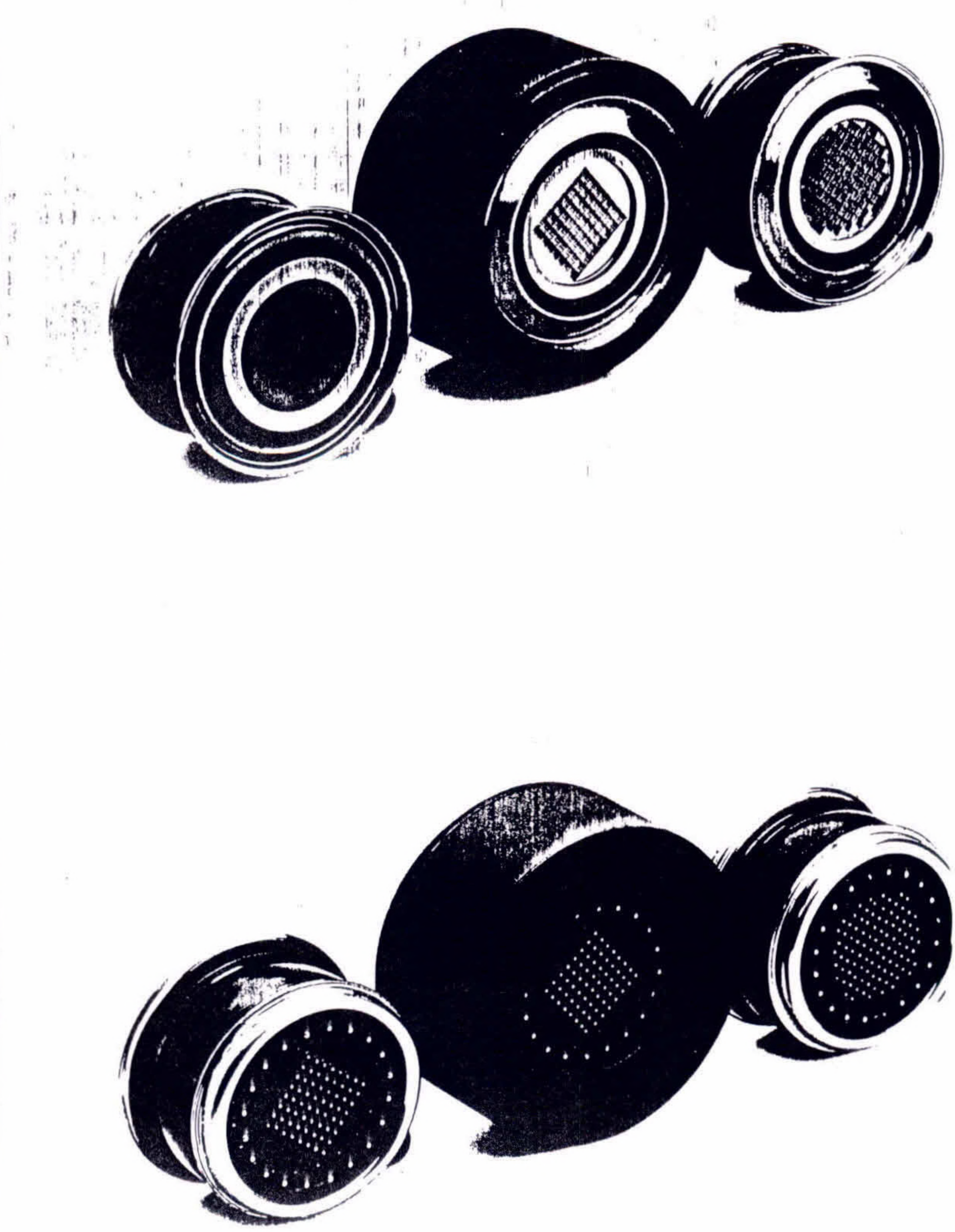

Selection of XP1700 family PMTs. *(top & bottom, l to r)* the XP1722, XP1702/A (a potted PMT) and XP1704.

A CLOSER LOOK AT A UNIQUE DESIGN

Figure 22 is a scanning electron micrograph of part of the first dynode foil of an XP1700 family PMT seen from the cathode. Clearly visible are details of the square dynode 'wells' (4 × 4 per channel) that collect and multiply the electrons. About 20% of the foil area is holes – an optimum value for this design. And virtually every electron passing through a hole is collected by the multiplier's second dynode foil owing to a patented dynode arrangement.* That's why this Philips Photonics' foil multiplier needs only ten stages to provide a gain of 10^6 at 1150 V. The multiplier's near-perfect collection efficiency, not only in the proximity-focused input stage but in subsequent stages too, provides a well-controlled, compact electron avalanche which gives very low inter-channel crosstalk.

Note that a foil dynode has a similar structure to a microchannel plate (as used in microchannel plate PMTs). The XP1700's foil-dynode stack therefore behaves like a *metal* microchannel plate which gives long operating life and a high output current.

Figure 23 shows one of the chemically-etched dynode wells in more detail. Also shown is one scanning line of the SEM electron beam across the well, and the response signal of the SEM detector along this line.

---

* Philips registered French patent 84200994.6, (1984), and extending to several countries.

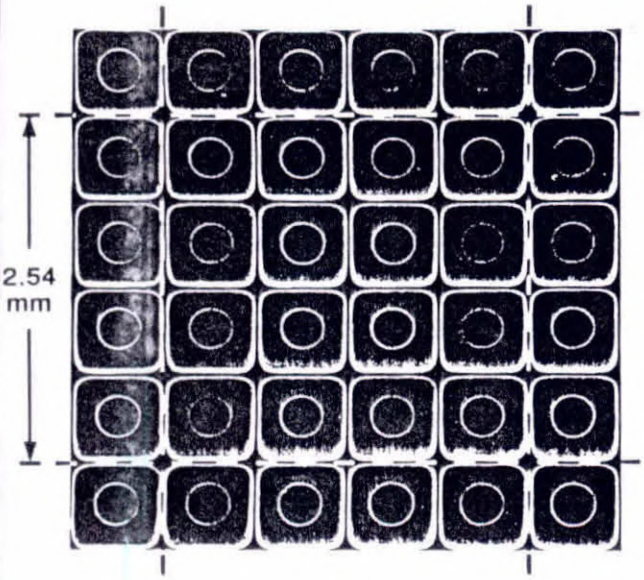

Fig.22 Part of a first dynode foil of an XP1700 family PMT. Magnification ×20 approx. The broken lines indicate pixel boundaries.

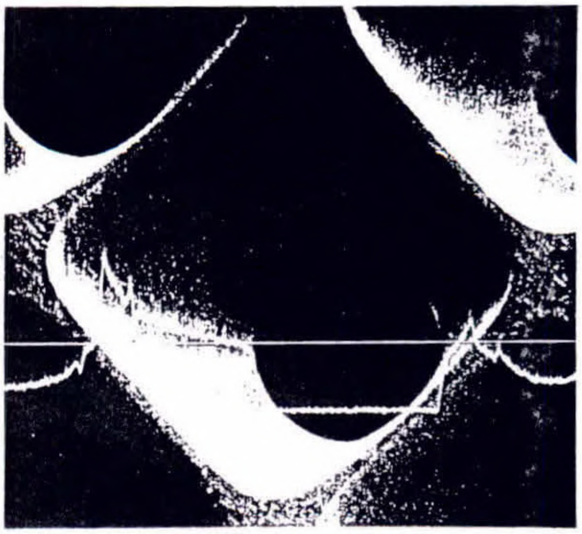

Fig.23 (centre) Detail of one foil well. Magnification ×80.

REFERENCES

1. BOUTOT J.P., et al., IEEE transactions on Nuclear Science NS-34, pages 449-452, 1987.
2. COMBY G. & MEUNIER R., Nucl. Instr. and Meth. A269, pages 246-260, 1988.
3. ERICSSON L., et al., IEEE transactions on Nuclear Science NS-34, pages 344-348, 1987.
4. LEBLANC M., et al., Nucl. Instr. and Meth. A273, pages 583-587, 1988.
5. BENDALI M., et al., Nucl. Instr. and Methods in Physics Research, A310, pages 373-378, 1991.
6. MAJEWSKI S., et al., Conference Records of the 1991 IEEE Nuclear Science Symposium & Medical Imaging Conference, Nov. 2-9, 1991, Santa Fe, New Mexico, USA; pages 324-330.
7. SALOMON M., Conference Records of the 1991 IEEE Nuclear Science Symposium & Medical Imaging Conference, Nov. 2-9, 1991, Santa Fe, New Mexico, USA; pages 346-348.
8. MATHIESON E., et al., Nucl. Instr. and Meth. No. 121, pages 139-149, 1974.
9. AGLIETTA M., et al., Imaging of Atmospheric EAS Cherenkov Light at EAS-TOP, Il Nuovo Cimento, Vol. 15C, N.3, 1992.

These references concern the XP4702 and XP4722 – predecessors of the XP1700 family. The XP1700 PMTs have improved cathode sensitivity and gain.

ACKNOWLEDGEMENTS

P. CUSHMAN of Yale University, USA, and T. MÜLLER of the University of California, USA for extensively testing various Philips Photonics multi-channel PMTs and granting permission to publish some of the results in this publication.

C. MORELLO and G. NAVARRA of the Istituto Nazionale di Fisica Nucleare (INFN), Italy for evaluating the use of a Philips Photonics multi-channel PMT in observing Cherenkov light from air-showers, and for granting permission to publish Figs. 17 and 18.

PHOTOMULTIPLIER TUBES
PRELIMINARY SPECIFICATION°

XP1752/D1

RED SENSITIVE 64- CHANNEL MULTI-ANODE TUBE

APPLICATIONS

For fibre read-out and rough imaging.

This tube allows the processing of 64 signals in parallel with less than 5 % cross-talk between channels. It is equivalent to 64 photomultiplier tubes but in a reduced volume.

GENERAL CHARACTERISTICS

					notes
Window					
Material			borosilicate glass		
Profile			plano-plano		
Refractive index at 400 nm			1.54		
Photocathode (Processed by transfer technology)			semi-transparent		
Material			standard multialkali photocathode		
Useful aera			20 x 20	mm^2	
Spectral range			270-800	nm	1
Wavelength for max. radiant sensitivity			500 ± 30	nm	
Radiant sensitivity at 500 nm	min : 50	typ :	60	mA/W	2 3
					3

Caution ! the voltage supply conditions may be such that one or both of the external metallic rings are connected to high voltage. Care should be taken to avoid electrical shock.

Characteristics for which typical and maximum (and/or minimum) values are given here will be measured for each individual tube and indicated on its test ticket. Other characteristics are approximate, i.e. checked by sampling.

° This document contains advance information. Specifications are subject to change without notice.

GENERAL CHARACTERISTICS (cont'd)

			notes
Multiplier			
First dynode	high-gain		
Structure	foil		
Number of stages	10		
Slope : log (gain)/log (supply voltage)	10		
Capacitances			
D10 (one pixel) to anode	2	pF	
D10 (one pixel) to all	2	pF	
anode to all	45	pF	
Output			
Segmented output electrode	last dynode		
Number of output channels	64		
Arrangement of output pins	8x8 matrix		
Pitch	2.54	mm	
Useful area of elements	2.54 x 2.54	mm	
Output pulse polarity	positive		

OPERATING CHARACTERISTICS with recommended voltage divider

				notes
For a gain of		1.0E+05		3 4
Supply voltage	max: 1150 V	typ : TBD		5
Anode dark current	max: 50 nA	typ : TBD		5 6
Anode pulse rise time		5	ns	7
Anode pulse duration (FWHM)		8	ns	7
Signal transit time		15	ns	7
Anode current linear within 2 % up to		10	mA	3
Output sensitivity uniformity				
Over 64 channels		max: 8:1		
Over at least 60 channels		max: 5:1		
Crosstalk between two adjacent channels		5	%	8
Life expectation (50% gain drop)		TBD		

* TBD : to be defined

LIMITING VALUES

Gain		max:1.E+06		3 9
Supply voltage		max:1400	V	
Total average anode current		max: 50	µA	3 10
Average current per output element		max: 5	µA	10
Voltage between photocathode and G1		max: 250	V	
Voltage between photocathode and D1	min :160	max: 250	V	
Voltage between anode and last dynode	min : 80	max: 125	V	11
Temperature range				
storage (less than 2 hours)	min :-30	max: +65	°C	
for continuous operation	min :-30	max: +50	°C	

RECOMMENDED VOLTAGE DIVIDER

Vd : arbitrary inter-electrode voltage unit

K : cathode
Dn : dynode n
A : anode

G1, G2 : focusing and accelerating electrodes

G1 and G2 can be used for gating operations

S1...S64 : output signals

RL1..RL64 : load resistors

Notes

With this voltage divider the multi-output collector D10 operates as a dynode and the output signals are positive.

By connecting the anode to a potential between that of D9 and that of the multi-output collector D10, the latter operates as an electron collector and the output signals are negative. In this case the gain is considerably reduced (by about a factor 6) as the gain of the last dynode is suppressed.

The grid G1 is internally connected to 4 pins on the base, each of them can be used.

The base metallic ring should preferably be at photocathode potential. However in order to minimize the noise level, it may be necessary to adjust its potential to a value between the potentials of the anode and cathode.

WARNING : The metal rings are connected to high voltage. Care should be taken to avoid electrical shocks.

CONNECTIONS

Cautions ! Do not deform the pins, especially the four tubular pins G1 by e.g. bending or filing.

Voltage divider

Extension pins are supplied with the tube for the connection to all electrodes.

Multi-output D10

- 8-pin extension strips are supplied with the tube.
- On top of those a 10x10 grid zip socket can be used. This accessory has to be ordered separately (see below).

ACCESSORY

FE4164 : Grid zip (zero insertion pressure) socket for 8x8 output.

REFERENCES

1- E.MATHIESON & al, Nuclear Instruments and Methods 121, pages 139 to 149,1974.

2- G.COMBY & al., Nuclear Instruments and Methods 217, pages 345 to 350, 1983.

3- J.P.BOUTOT & al., IEEE Transactions on Nuclear Science NS-34, p.449-452,1987.

4- L. ERICSSON & al., IEEE Transactions on Nuclear Science NS-34, p. 344-348,1987.

5- G.COMBY & R. MEUNIER, Nucl. Instr. and Meth. A269, pages 246 to 260, 1988.

5- M.LEBLANC & al., Nucl. Instr. and Meth. A273, pages 583 to 587, 1988.

Note : These papers concern the previous versions XP4702 and XP4722 of this tube family that showed somewhat lowers performances in terms of cathode sensitivity and gain.

1- The spectral range is defined between the minimum and maximum wavelengths for which the radiant sensitivity is 1/100 of its peak value.

2- Radiant sensitivity (expressed in mA/W) is measured with a tungsten filament lamp with a colour temperature of 2856 ± 5 K. Light is transmitted through an interference filter.

3- Average value over the 64 pixels.

4- Measured at the anode. Gain measured at D10 is slightly lower (roughly by a factor 0.9).

5- Whenever possible, the power supply should be arranged so that the cathode is earthed and the anode is at +HT. However it is sometimes necessary to supply the tube with the anode earthed and the cathode at -HT. Under these circumstances noise and dark current will generally increase and become erratic, particulary after application of voltage ; the glass envelope of the tube should be supported only by insulators with an insulating resistance greater than 10.E+15 ohms ; if a metal shield is used, this should be kept at cathode potential.

6- Dark current is measured at ambient temperature, after the tube has been in darkness for approximatively 1 min. Lower value can be obtained after a longer stabilization period in darkness (approx. 30 min.).

7- Measured with a pulse source, with a pulse duration (FWHM) below 1 ns, the cathode being completely illuminated. The rise time is determined between 10 % and 90 % of the anode pulse amplitude. The signal transit time is measured between the instant at which the illuminating pulse of the cathode becomes maximum, and the instant at which the anode pulse reaches its maximum. Rise time, pulse duration and transit time vary with respect to high tension supply voltage V_{ht} as $Vht^{-1/2}$.

8- The tube is exposed to a 1 mm diameter parallel light beam centered on the pixel to be tested. The currents of this pixel and one of the adjacents ones are recorded. The crosstalk is given by the percentage of those two values. For reading-fibres directly coupled to the window, the crosstalk increases markedly for a fibre diameter > 500 µm. In such a case it is advantageous to use a version which includes a fibre input plate as window and provides a low cross talk (<6 %) up to a 2 mm fibre diameter.

9- The voltage corresponding to this maximum gain is equal to 1.25 times the voltage indicated on the test ticket of the tube. The max gain can not be reached if this required voltage is higher than the supply voltage limiting value.

10- A total average anode current less than 10 µA together with an average current per output element less than 1µA is recommended for applications requiring good stability and long life.

11- When calculating the anode voltage, the voltage drop across the load resistor should be taken into account.

XP1752/D1

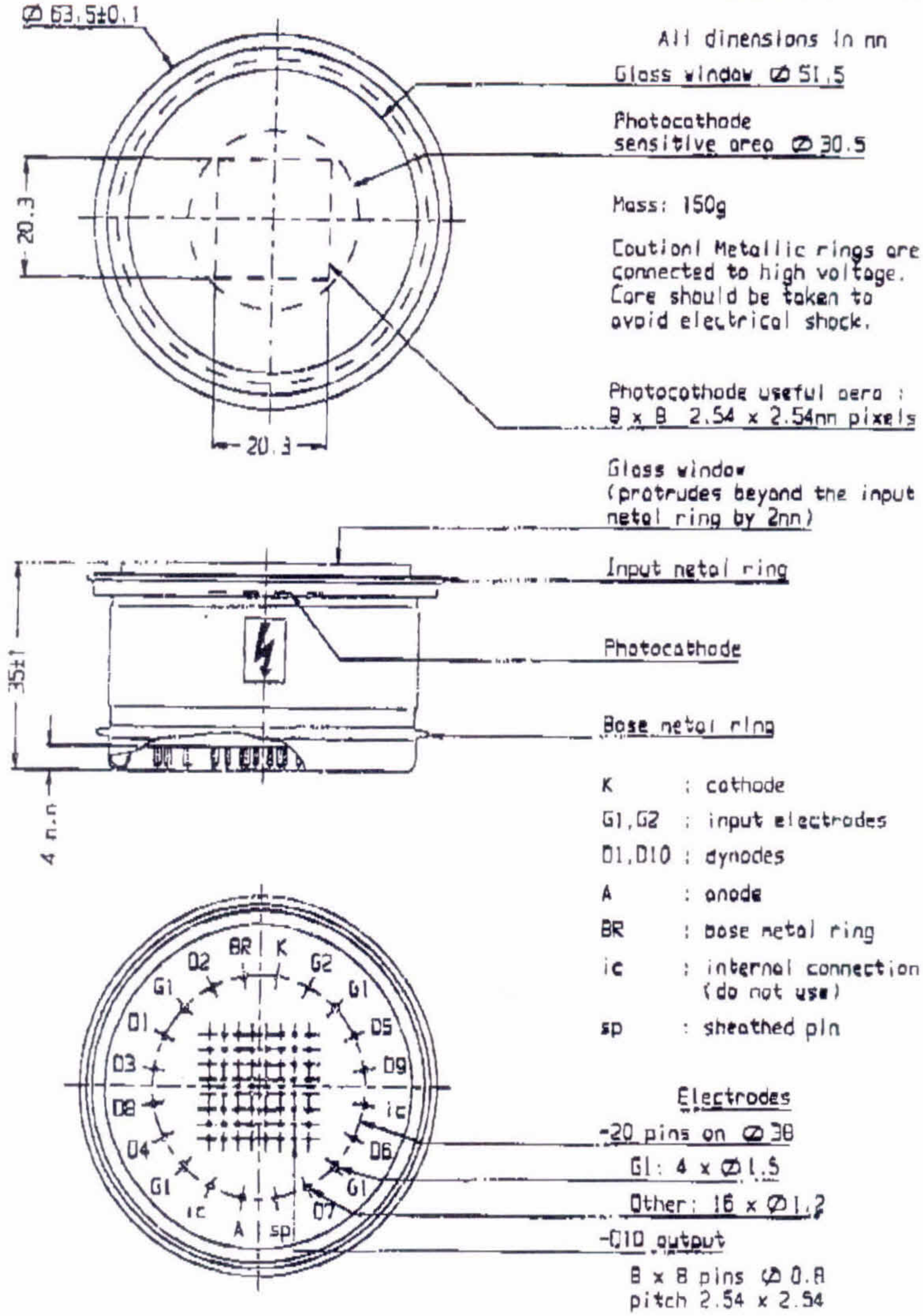

All dimensions in mm

Glass window Ø 51.5

Photocathode sensitive area Ø 30.5

Mass: 150g

Caution! Metallic rings are connected to high voltage. Care should be taken to avoid electrical shock.

Photocathode useful area : 8 x 8 2.54 x 2.54mm pixels

Glass window (protrudes beyond the input metal ring by 2mm)

Input metal ring

Photocathode

Base metal ring

K	: cathode
G1,G2	: input electrodes
D1,D10	: dynodes
A	: anode
BR	: base metal ring
ic	: internal connection (do not use)
sp	: sheathed pin

Electrodes

-20 pins on Ø 38

G1: 4 x Ø 1.5

Other: 16 x Ø 1.2

-D10 output

8 x 8 pins Ø 0.8
pitch 2.54 x 2.54

94-04-20 Rev : 0 Drawing 99900333 Page: 1/1

Philips
Photonics

PHILIPS

Referências

Camp91 D. O. Campos; "Formierung von Plasmakonfigurationen mit negativ eingefangenem magnetfeld in verschiedenem gasen"; Tese de Doutorado, Bochum 1991

DeSi70 A. W. De Silva, G. C. Goldenbaun; "Methods of Experimental Physics"; Academic Press, vol. 9, cap. 3, 1970

Kunz68 H J. Kunze; in "Plasma Diagnostics"; ed. W. Lochte-Holtgreven, North Holland, amsterdan, pag. 550, 1968

Larr59 R. D. Larrabee; Journ. of the Optical Society of America, 49 nr. 6, 1959

Long77 D. A. Long; "Raman Spectroscopy"; McGraw-Hill, 1977